To the Graduate Council:

I am submitting herewith a thesis written by Janna Peevler entitled "Sulfur Isotope Microanalysis of Sphalerite by SIMS: Constraints on the Genesis of Mississippi Valley-type Mineralization from the Mascot-Jefferson City District, East Tennessee." I have examined the final structure of this thesis for form and content and recommend that it be accepted in partial fulfillment of the requirements for the degree of Master of Science, with a major in Geology.

Kula C. Misra

Kula C. Misra, Major Professor

We have read this thesis and
recommend its acceptance:

Accepted for the Council:

Interim Vice Provost and Dean of the
Graduate School

Sulfur Isotope Microanalysis of Sphalerite by SIMS: Constraints on the Genesis of Mississippi Valley-Type Mineralization from the Mascot-Jefferson City District, East Tennessee

A Thesis
Presented for the
Master of Science Degree
The University of Tennessee, Knoxville

Janna L. Peevler
August, 2001

Dedication

To my parents,
Dean and Leslie Peevler and
Albert and Sharon Norris,
who have been so supportive and patient
throughout this endeavor.

Acknowledgements

I have so many people to thank for their assistance during my tenure in graduate school. I am grateful to my advisor, Dr. Kula C. Misra, for helpful suggestions and discussion but mostly for letting me do things my way. I'd also like to thank my other committee members, Dr. Claudia I. Mora and Dr. Harry Y. McSween, Jr. for helpful discussions and suggestions toward completion of the research and the writing of this thesis.

There are quite a number of people who have provided technical guidance during the data collection phase of my thesis. I am grateful to the Oak Ridge National Lab, Dr. Lee Riciputi and Dr. Mostafa Fayek for gracious use of their laboratory for data collection. I am especially indebted to Mostafa for his assistance in data collection as well as his helping me unravel an extremely complex problem. I surely wouldn't have been able to complete this thesis without his assistance. Also I would like to thank Dr. Larry Taylor and Dr. Allen Patchen for assistance on the electron microprobe.

Financial support has been provided by a number of sources. The University of Tennessee Geological Sciences Department provided primary support. The Athletic Department and the University Honors Program provided financial support during the lean times. A research grant from the Geological Society of America helped defray the costs associated with data collection.

A special thanks to Melody, Denise and Teresa for all the good cheer they brought me. Marvin Bennett has been especially helpful with all things technical and computer related.

Graduate school wouldn't have been bearable without all the friends I've made during my time here. The WIGS (Women In Geology) - Amy, Dana, Heather, Sandra, Valerie, Sara, Karen, and Wendy - have provided a supportive and fun environment. The folks in the Hatchery are most appreciated - Scott "swilli" Williams, Jen and Chris Whisner and my could-be brother, Joe Hill. Dave King and Peter Nester provided enduring wit and wisdom. My hip sister Elizabeth provided hours and hours of procrastination and shopping therapy, and also helped me keep my eye on the Target. And finally to my dearest Nate who never quit believing in me or cheering for me, this feat would have been nearly impossible without you.

Abstract

The Mascot-Jefferson City district is the most productive zinc district in East Tennessee. The deposits are of the Mississippi Valley-type (MVT), hosted by carbonate rocks and dominated by sphalerite mineralization in strata-bound breccia bodies. We have utilized the high spatial resolution (20-30 μm) of the ion microprobe to obtain *in situ* sulfur isotopic analyses from discrete growth zones in sphalerite and analyses of associated pyrite.

Two types of pyrite were noted: pre-sphalerite, diagenetic pyrite ($\delta^{34}S$ = -16.1‰ and -20.0‰) and syn-sphalerite pyrite that is intergrown with sphalerite ($\delta^{34}S$ = 31.3‰ to 33.7‰). Sulfur isotope geothermometry on one sphalerite-pyrite pair yielded a temperature of 149° ± 31°C, which is consistent with fluid inclusion estimates of 141° ± 54°C (average 139.2 °C). Two textural varieties of sphalerite mineralization (zoned and unzoned) were characterized. Zoned sphalerite exhibits fine (μm to cm) banding that has grown around a carbonate substrate. Zoned sphalerite has $\delta^{34}S$ values from 27.8‰ to 51.0‰, high Cd contents (up to 0.96 wt. %) and dark areas that are likely due to minute inclusions of organic carbon. The unzoned sphalerite has $\delta^{34}S$ values from 20.2‰ to 39.5‰, high Fe content and no organic inclusions.

Regardless of the textural variety of sphalerite mineralization, our results show that the sulfur isotopic composition of sphalerite within a single polished

thin section is heterogeneous and can vary by as much as 15‰. The $\delta^{34}S$ values recorded in this study are among the heaviest ever reported for MVT sphalerite. The micro-scale $\delta^{34}S$ variations and presence of such high $\delta^{34}S$ values have not been previously documented for east Tennessee. The data presented here suggests multiple sulfur sources and complex precipitation mechanisms. Several possible mechanisms are examined. The most probable scenario involves significant sulfur input from a sulfate- and metal-bearing fluid of variable $\delta^{34}S$ composition mixing with a gas cap containing H_2S of relatively homogeneous $\delta^{34}S$ composition. The gas cap provided lesser amounts of sulfur to the system. Mixing of two isotopically different sulfur sources of variable proportions can account for the observed microscale variation in $\delta^{34}S$ (sphalerite).

Table of Contents

List of Tables

List of Figures

Chapter One

Introduction

Zinc mineralization of varying intensity occurs throughout the southern Appalachians in Cambrian and Lower Ordovician carbonate units. The Mississippi Valley-type (MVT) deposits of East Tennessee, which have been producing zinc for over 150 years, currently contribute approximately 20% of the United States zinc production. The two major stratigraphic units that host all of the significant mineralization in East Tennessee are the Lower Cambrian Shady Dolomite and the Lower Ordovician Upper Knox Group (Kingsport Formation and Mascot Dolomite). Although the mineral paragenesis varies among deposits and mining districts, the overall ore-gangue assemblage, consisting of highly variable proportions of sphalerite, galena, barite, fluorite, sparry dolomite and sparry calcite, is typical of carbonate-hosted MVT deposits. The zinc deposits of East Tennessee are characterized by very low Pb: Zn ratio and represent the zinc-rich end member of the spectrum of MVT deposits (Sangster, 1983).

Ore-forming fluids in East Tennessee were basinal brines that either migrated up dip due to compaction by overlying sediments (Jackson and Beales, 1967) or were driven by gravity as a consequence of uplift (Garven and Freeze, 1984). Despite numerous earlier studies (e.g., Churnet and Misra, 1983; Haynes et al., 1987, 1989; Jones, 1993; Appold et al., 1995), the sources of metals, sulfur, and brines, the mechanism of sphalerite precipitation, and the extent of regional

fluid flow are poorly constrained. One group of models advocates simultaneous transport of both metal cations and sulfur to the site of deposition (e.g., Giordano and Barnes, 1979; Sverjensky, 1984; Haynes et al., 1989). The other model envisages the transport of sulfur and metal cations in different fluids, and mixing of the fluids at the site of sulfide deposition (Anderson, 1973, 1983; Jones, 1993; Taylor et al., 1983).

Bulk sulfur isotopic analyses of sulfides have been used to constrain the genesis of MVT deposits (e.g., Kesler et al., 1994; Jones, 1993). Jones (1993) reported bulk sulfur isotope values ranging from 27.6‰ to 36.1‰ for the Mascot-Jefferson City district, and attributed mineralization to interaction of metal-bearing brines with a sour gas cap. Bulk isotopic analyses provide important information on a regional scale; however, *in situ* microanalysis can detect isotopic variations within a single zoned crystal, and, therefore can potentially provide more detailed information on the mechanism of precipitation as well as distinguish among multiple fluid events that may have been associated with complex zoned textures. The complex zoning textures in East Tennessee ores require an analytical technique with high spatial resolution of sulfur isotopic data. An increasing number of ion and laser probes in geological laboratories have facilitated the routine application of *in situ* stable isotopic microanalysis to problems in exploration geochemistry and ore genesis (e.g., Deloule et al., 1986; Layne et al., 1991; McKibben and Eldridge, 1995; Fayek et al., 2000). In this

study, a CAMECA 4f ion microprobe (secondary ionization mass spectrometer, SIMS) was used to determine the *in situ* micro-scale sulfur isotopic variations associated with zoned sphalerite.

Chapter Two

Geologic Setting

The East Tennessee carbonate-hosted, Mississippi Valley-type deposits are located in the northeastern part of Tennessee within the Appalachian Valley and Ridge physiographic province (Figure 1). The Valley and Ridge province lies between the Blue Ridge to the southeast and the Appalachian Plateau to the northwest. The Valley and Ridge consists of a thick sequence of epicontinental basin sediments that accumulated during the Cambrian and Ordovician (Hatcher and Odum, 1980; Shanmugam and Lash, 1982). The area contains multiple northwest-southeast trending thrust faults that occurred during the Alleghenian orogeny.

The zinc deposits are hosted by the Lower Ordovician upper Knox Group, which represents a peritidal to subtidal environment of deposition (Churnet et al., 1982). The Knox Group is divided into four formations (Harris, 1969) - Copper Ridge Dolomite, Chepultepec Dolomite, Kingsport Formation and Mascot Dolomite (Figure 2).

The Kingsport Formation is predominantly a medium- to coarse-grained dolostone and limestone, with some lenses of fine-grained dolostone. The limestone was deposited in a subtidal environment and was subsequently partially dolomitized on a regional scale. The Mascot dolomite is predominantly a fine-grained dolostone, with some coarse-grained dolostone, and occasional

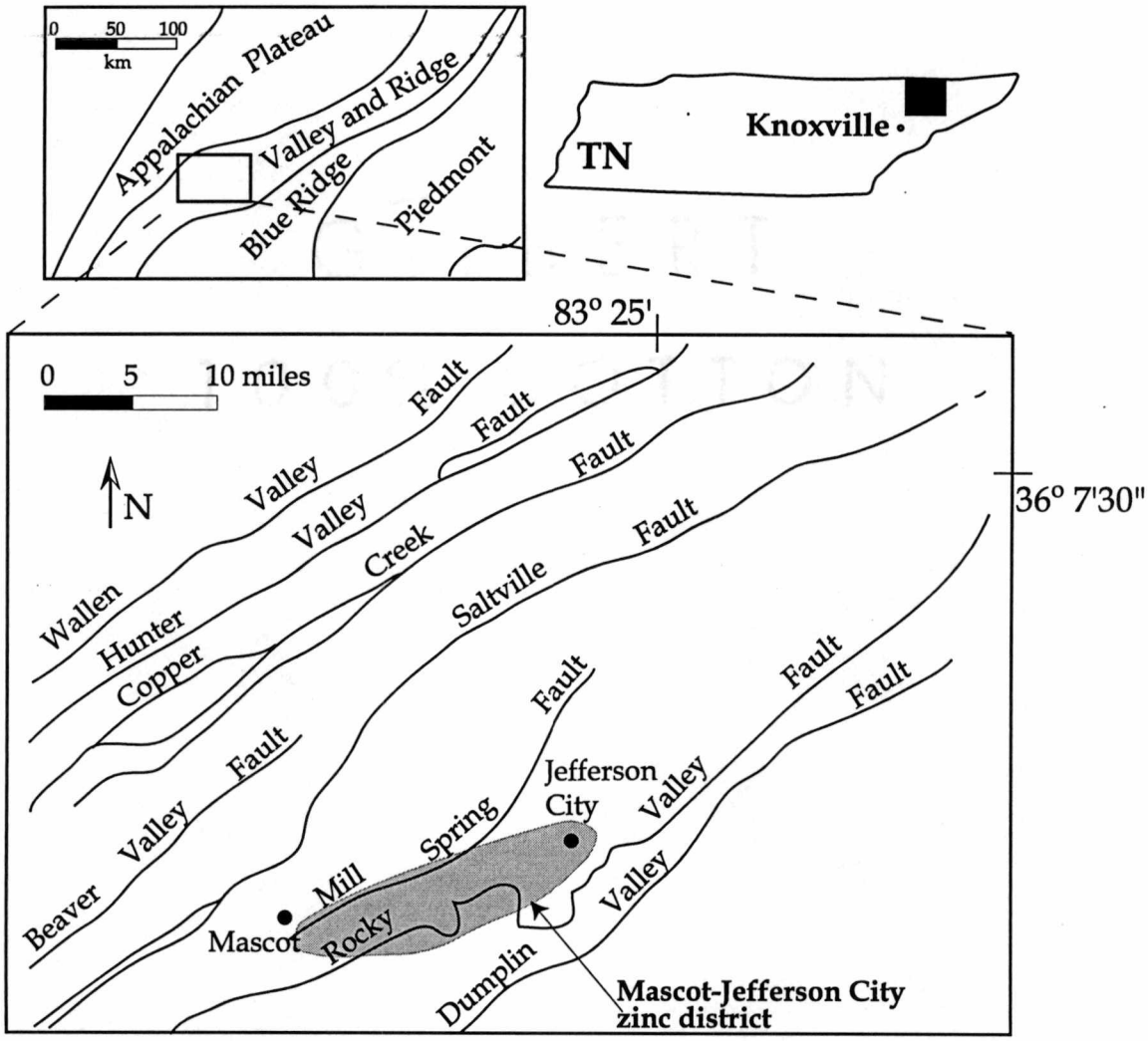

Figure 1. Generalized structural map of the Mascot-Jefferson City zinc district (After Hill, 1971).

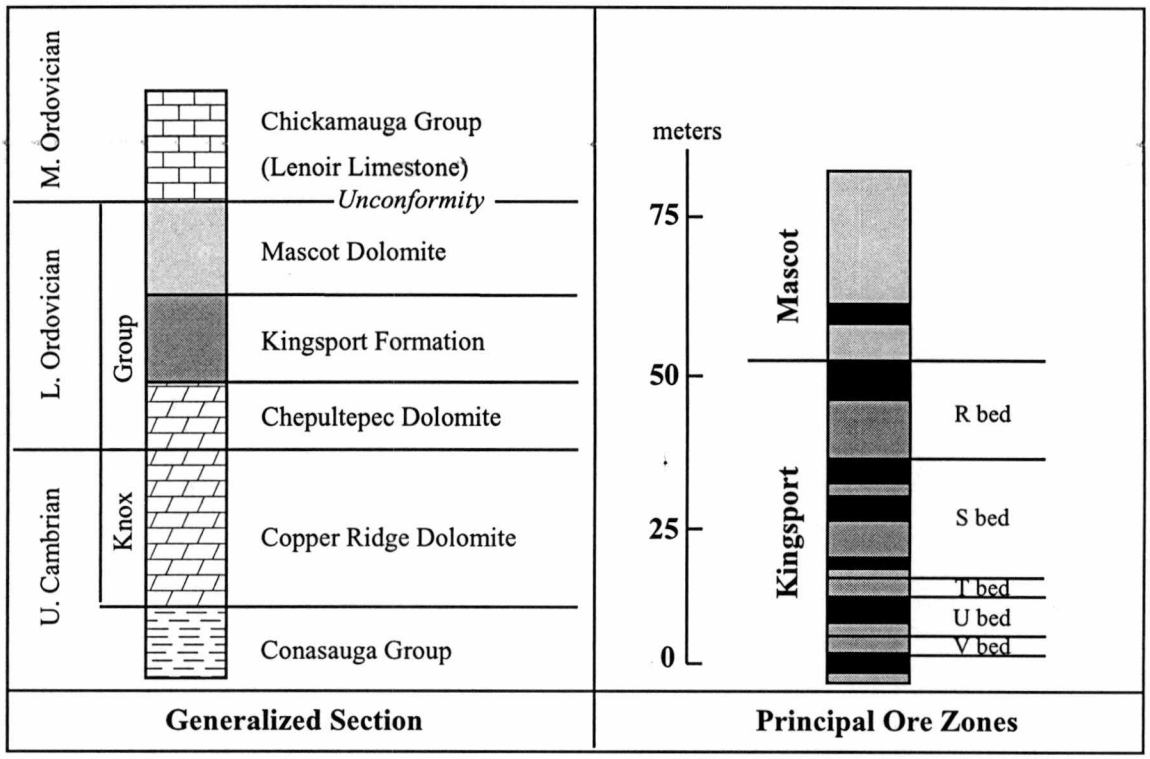

Figure 2. Generalized stratigraphy of the Mascot-Jefferson City zinc district, East Tennessee, with principal ore horizons. The column on the right represents the interval of mineralization with the principal ore horizons noted in solid black. The alphabetic designation of the subunits (Q, R. S. T. U, V) is after the nomenclature of the New Jersey Zinc Company. Most of the commercial ore is found within the U, S, and R beds in the Kingsport and lowermost part of the Mascot Dolomite (After Crawford et al., 1969).

lenses of brownish limestone. The Mascot represents a supratidal to intertidal depositional environment, and the units together represent a coastal flat and adjacent shallow marine environment. Zinc mineralization occurs in the lower fifth of the Mascot Dolomite and the upper half of the Kingsport Formation, with most economic ore localized near the boundary between the two units (Hill, 1971). The Mascot is separated from the overlying Middle Ordovician Chickamauga Group by an erosional surface, locally referred to as the post-Knox Unconformity, which was likely caused by uplift of the platform (Shanmugam and Lash, 1982). The post-Knox Unconformity represents subaerial exposure and was formed when water receded exposing the top of the Knox Group. This exposure led to development of karst topography and the formation of a regional paleoaquifer system in the units below that would later host zinc mineralization (Harris, 1971).

The zinc ore in the district is hosted within crackle and rubble breccias, predominantly as open-space fillings (Figure 3). Better grades of mineralization are almost always associated with rubble breccias (in which fragments show significant movement and rotation); crackle breccias (in which breccia fragments show little or no displacement) are much less intensely mineralized (Hoagland et al., 1965; Crawford et al., 1969). Breccia bodies in the district apparently resulted from the collapse of overlying strata due to dissolution of limestone in the Kingsport Formation (Harris, 1969, 1971; Crawford et al., 1969; Wedow and

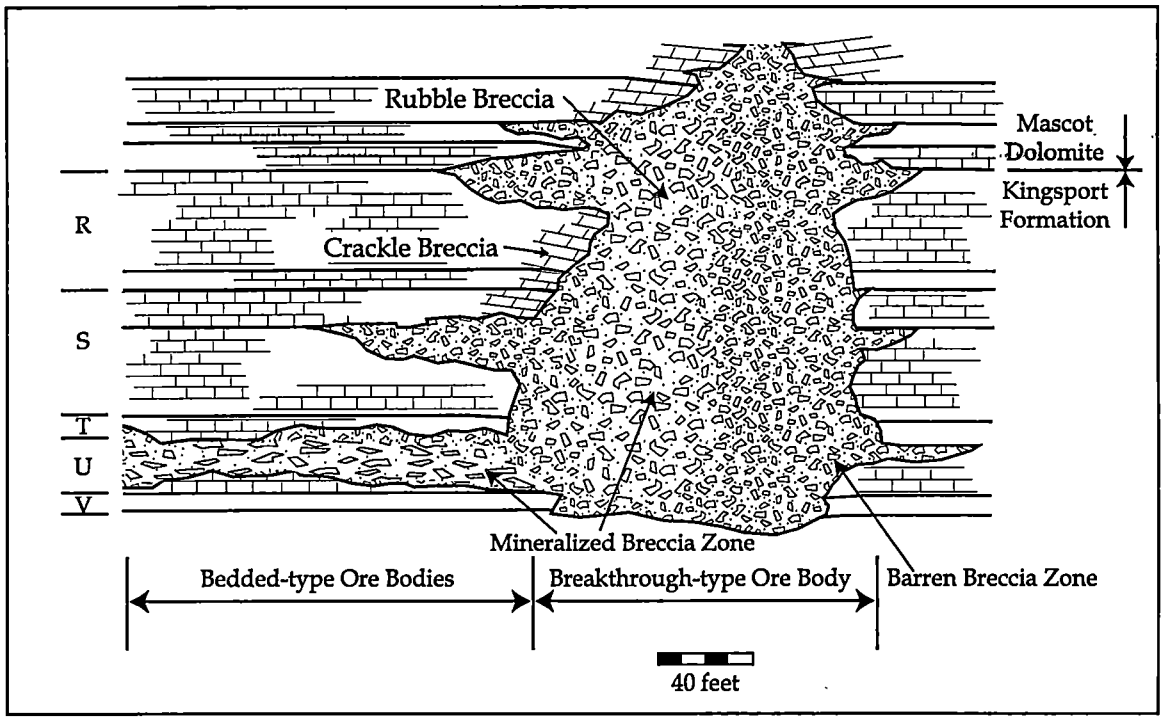

Figure 3. Cross section through a typcial collapse breccia body. The relationship between breakthrough and bedded mineralized structures was first described by Crawford et al., (1969). The nomenclature of ore horizons are the same as noted in Figure 3. After Crawford et al., 1969.

Harris, 1971) and may be one of two forms (Figure 3): breakthrough structures, which may cut across one or more stratigraphic horizons; and bedded structures that are confined to individual beds (Hoagland et al., 1965). Breccia bodies likely developed along faults that pre-dated mineralization but the relationships are obscured due to post-mineralization movements along these zones (Hoagland et al., 1965; Crawford et al., 1969).

Based on radiometric dating of wall rock, Kesler et al. (1988) proposed that the source of sulfur was basinal brines from the Ordovician Sevier basin (Figure 4) and underlying Cambrian to Lower Ordovician sediments. Strontium isotope analysis of dolomite gave an age of 405-320 Ma, suggesting a correlation of zinc mineralization with the Acadian orogeny (Kesler et al., 1988). Rb-Sr dating of sphalerites from the Mascot Jefferson City district yielded dates of 406-327 Ma. (Nakai et al., 1990, 1993). At this time, the shales of the Sevier basin are estimated to have been buried to a depth of 5-6 kilometers and attained a temperature of approximately 200 °C (Walker and Foreman, 1990).

East Tennessee hosts six ore districts of varying size: Powell River, Evanston, Embreeville, Copper Ridge, Sweetwater, and Mascot-Jefferson City (MJC) district. The two most productive districts, Mascot-Jefferson City and Copper Ridge, are shown in Figure 4. This study focuses solely on the Mascot-Jefferson City district, which is the largest of these districts.

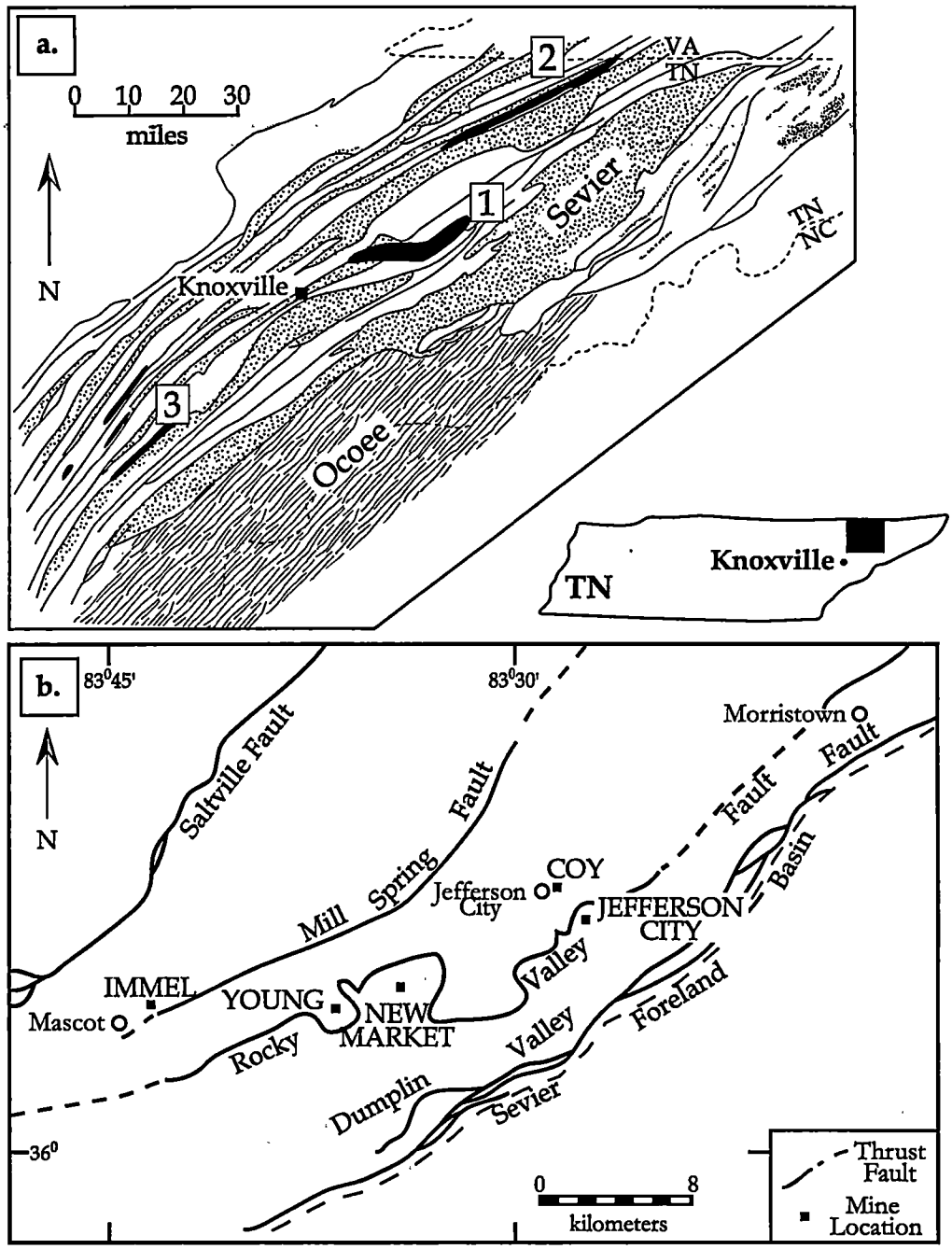

Figure 4. Regional and local maps of East Tennessee. a. Locations of the three important MVT districts in East Tennessee in relation to the basins that probably provided mineralizaing brines. MVT deposits shown in black are: 1 - Mascot-Jefferson City zinc district, 2 - Copper Ridge zinc district, 3 - Sweetwater barite-fluorite district. The present location of the Sevier basin is shown with a stippled pattern, and the Ocoee basin is shown with a wavy pattern (after Kesler et al., 1988); b. Locations of the mines within the Mascot-Jefferson City district (Hill, 1971).

The MJC district contains abundant zinc mineralization with sphalerite as the dominant ore mineral and sparry dolomite as the dominant gangue mineral (commonly referred to as "white gangue dolomite"). Other gangue minerals include minor amounts of pyrite and marcasite and very small amounts of fluorite, quartz and calcite. Galena has been observed only in trace amounts. One exception is the Immel mine, which has a small amount of galena associated with the sphalerite ore. Sphalerite is generally light colored (honey yellow to brown) with a relatively low in Fe content (usually < 1%) (Churnet and Misra, 1983).

Chapter Three

Methods of Study

Recent advances in mass spectrometry allow a more detailed examination of a variety of geologic materials. In contrast to traditional mass spectrometry methods, ion microprobe analysis provides fine-scale (<50μ) spatial resolution of isotopic variations. This technique eliminates the need for drilling through a specimen or physical separation of minerals for analysis, and subsequent destruction of the material used for analysis. With the ion microprobe technique, textural relations are preserved and can be re-examined after the analysis (Riciputi et al., 1998). This technique has been used by many workers (e.g. Deloule et al., 1986; McKibben and Eldridge, 1995) to examine sulfur isotope zoning in other MVT deposits. Deloule et al. (1986) performed analysis on two galena crystals from Viburnum Trend, southeast Missouri and found that the crystals exhibited oscillatory zoning in both lead and sulfur isotopes, suggesting discontinuous input of both lead and sulfur. McKibben and Eldridge (1995) also found sulfur isotopic variations in sphalerite and galena that were related to the paragenesis of the deposits, indicating that the fluid was changing in chemistry throughout sulfide deposition.

For this study, samples were collected from the New Market mine, and samples from other mines (Young, Jefferson City, and Coy) were selected from the Economic Geology collection maintained at the Department of Geological

Sciences of the University of Tennessee, Knoxville. The goal was to incorporate selected samples from several mines so that chemical and isotopic compositional variations could be studied in sphalerites displaying a variety of textural relationships. The sphalerite textures represented by these samples include open space filling, color banding, and rosettes.

Petrography

Polished thin sections of the samples were examined under plane-polarized light as well as reflected light to determine the textural relationships of ore-gangue minerals, paragenesis, and the presence of fluid inclusions.

Electron Microprobe Analyses

Chemical compositional data were obtained with the electron microprobe (automated Cameca SX-50) at the University of Tennessee. Analyses were performed using an accelerating voltage of 20 keV, a beam diameter of 5 μm, a beam current of 20 nA, and counting times of 20 s per element. The elements analyzed were S, Fe, Zn, Mn, Cu and Cd and detection limits for these elements were on the order of 0.05 wt. %. ZAF (PAP) corrections adapted for the Cameca probe were applied to all analyses to reduce the data. Traverses were made across selected polished sections to note any significant changes in the amount of Fe or Cd. Backscatter electron images were taken to determine if compositional changes could be responsible for color banding.

The sections were then re-polished and cleaned to remove the carbon coating. A ~200 Å thick Au coat was sputter-deposited on the sample mount surface prior to ion microprobe (SIMS) analysis. The mounts were placed in steel sample holders where surface conductivity was approximately 5-10 ohms/cm. The entire assembly was then placed in the ion microprobe sample lock and held at high vacuum for a minimum of 8 hours prior to the start of analysis.

Ion Microprobe (SIMS) Analyses

The analytical protocol for S-isotope measurements in sphalerite using the CAMECA ims 4f ion microprobe at Oak Ridge National Laboratory was similar to that described by Riciputi (1996). Sulfur isotope ratios ($^{34}S/^{32}S$) in sphalerite were measured using a Cs^+ primary beam and monitoring S^- secondary ions with extreme energy filtering of 200 eV. A normal incidence flood gun was employed to neutralize potential sample charging. The ~3 nA primary ion beam was focused to a 15 x 30 μm spot using a 100 μm aperture in the primary column. Secondary sulfur ions were detected sequentially by switching the magnetic field. The detection system consisted of a Balzers electron multiplier coupled with an ion counting system with an overall dead time of 8.5 ns. A typical analysis lasted ~15 minutes, comprising 100 analysis cycles.

During the isotope measurement process by ion microprobe, an intrinsic mass dependent bias is introduced and is referred to as instrumental mass fractionation (IMF). A variety of processes combine to produce the observed

IMF. These include secondary atom extraction (sputtering) and ionization, (Shroeer et al., 1973; Williams, 1979, Yu and Lang, 1986), secondary ion transmission (Shimizu and Hart, 1982), and detection (Valley and Graham, 1991, Lyon et al., 1994). The greatest contributors to the IMF are sputtering and ionization, which depend most strongly upon sample characteristics (i.e., chemical composition). This is referred to as compositionally dependent fractionations or "matrix effects" (e.g., Valley et al., 1997). Therefore, in ion microprobe analysis, IMF is corrected for by comparing measurements of a chemically and isotopically homogenous mineral standard that is compositionally similar to the unknown. Ion microprobe results from the standard are compared to its accepted isotopic composition in order to compute a correction factor that is applied to the unknowns measured during the same analysis session (e.g., Leshin et al., 1998). The standards used in this study were Balmat sphalerite (+14‰ CDT) and Balmat pyrite (+14.6‰ CDT) from the Balmat mine, New York (Crowe et al., 1996).

The overall precision and accuracy (relative to the standard) of each isotope analysis includes errors arising from counting statistics of each individual analysis, calibration to a known standard, and uncertainty in deadtime corrections arising from variable count rates. In general, the overall analytical precision was ±0.8‰. Values are reported in ‰ relative to Canyon

Diablo Troilite (CDT). Sources of error in the SIMS analyses are further addressed in Appendix B.

Fluid Inclusion Microthermometry

Twenty doubly polished sections of sphalerite samples, including those used for electron microprobe and SIMS analyses, were prepared for fluid inclusion analysis. This study examined only primary inclusions in sphalerite. Primary inclusions are inclusions that were trapped during crystallization and, therefore, represent the fluid from which the sphalerite precipitated. A complete list of criteria for determining whether an inclusion is primary or secondary is given in Roedder (1984). In this study, inclusions that were randomly distributed or separate from other inclusions were assumed to be primary. Inclusions aligned in planes were assumed to be secondary and were not used.

Microthermometric analyses of fluid inclusions were done at the University of Tennessee on a Fluid, Inc. version of the U.S.G.S. gas flow heating/freezing system. Synthetic inclusions of pure H_2O and $H_2O + CO_2$ with 25% CO_2 were used for calibration of the instrument. Temperature measurements are reproducible to ±3.0°C. The measurement on each inclusion was subjected to at least one repetition to insure reproducibility of the data. In order to keep thermal gradients to a minimum, the sample was kept in direct contact with the thermocouple and a constant flow of N_2 gas around the sample was maintained during each experiment.

Heating and freezing runs were performed to record several phase-transition temperatures. Freezing runs were performed first so that the inclusion would not be stretched or disturbed by the heating process, rendering it unusable for the freezing run. The temperature of first melting (T_e) is the temperature at which the first ice melting occurs following complete freezing of the inclusion. The freezing temperature (T_m) is the temperature of final melting of ice and this temperature is useful for determining salinity. The homogenization temperature (T_h) is the temperature at which the vapor and liquid phases in the inclusion homogenize to produce a single-phase fluid. It represents the minimum temperature at which the fluid was trapped. The data were not corrected for pressure.

Chapter Four

Results

Petrography

Sphalerite mineralization occurs predominantly as open space fillings within breccia bodies, but with a variety of textures (see Appendix A for a summary of all the hand specimens studied). For convenience of discussion, the observed sphalerite textures may be divided into two descriptive categories: a. relatively homogeneous and (apparently) unzoned (Figures 5a, b); and b. color banded or zoned (Figures 5c, d). The unzoned, honey-yellow sphalerite, the most common textural variety, occurs on several scales: large masses, fracture fillings, or small veinlets. Reflected- and transmitted-light microscopy show that this sphalerite has no obvious zoning, has less organic inclusions, and is practically devoid of pyrite. Zoned sphalerite consists of concentric bands of honey-yellow sphalerite alternating with bands of darker green or brown, coarse-grained sphalerite. The dark bands have been attributed to minute inclusions of organic carbon (Craig et al., 1983; Kettler, 1990). The rosette shape is a subset of the zoned sphalerite in which the bands occur as concentric rings.

Pyrite is not common in these deposits but was found in some specimens as small (50 μ) irregular pyrite crystals within the host dolostone (Figure 6a). This pyrite clearly unrelated to breccia-fill sphalerite precipitation and is interpreted to be diagenetic (pre-ore). In some specimens, however, pyrite is

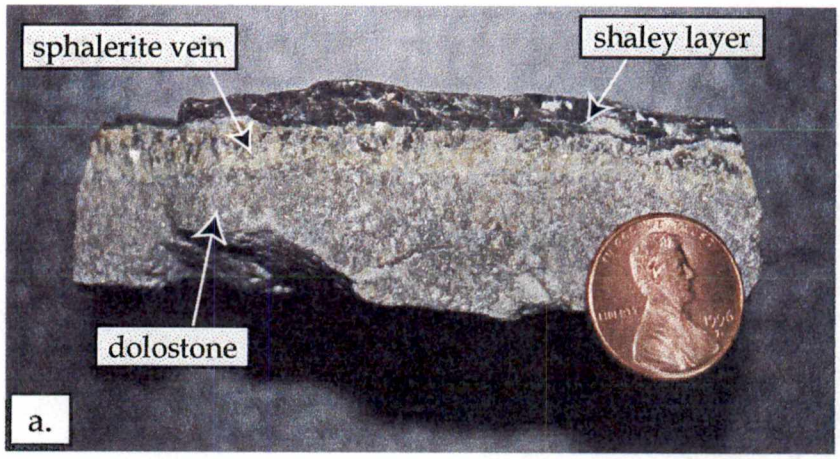

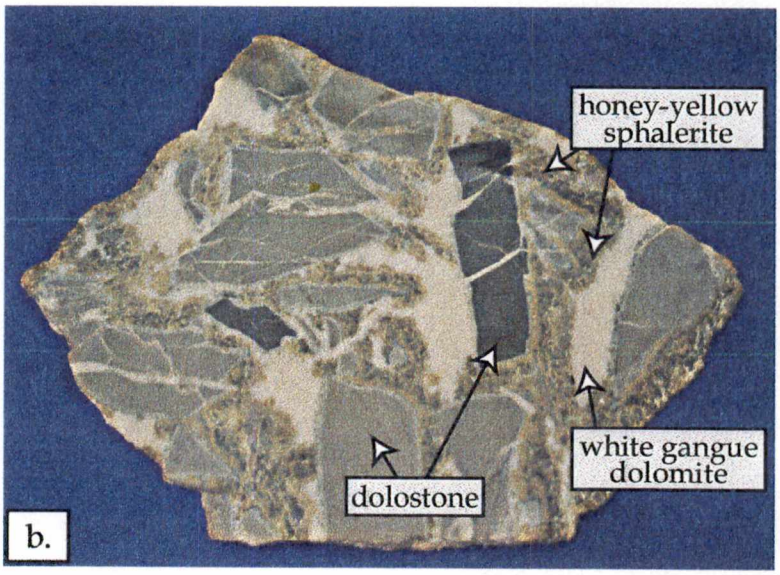

Figure 5. Sphalerite textural varieties, Mascot-Jefferson City zinc district, East Tennessee. a. Fracture-fill, honey yellow sphalerite veinlet bounded by Kingsport dolostone and a shaley layer (sample jp2, New Market mine); b. honey-yellow unzoned sphalerite with white gangue dolomite and dolostone breccia fragments (Beaver Creek mine); c. sphalerite rosettes (Young Mine) with concentric rings of light and dark color sphalerite precipitated on the surface of a dolostone breccia fragment with white gangue dolomite; d. color banded sphalerite (Coy mine) with bands of honey yellow sphalerite and dark green to brown sphalerite with white gangue dolomite and sand-size internal sediment including fine-grained sphalerite.

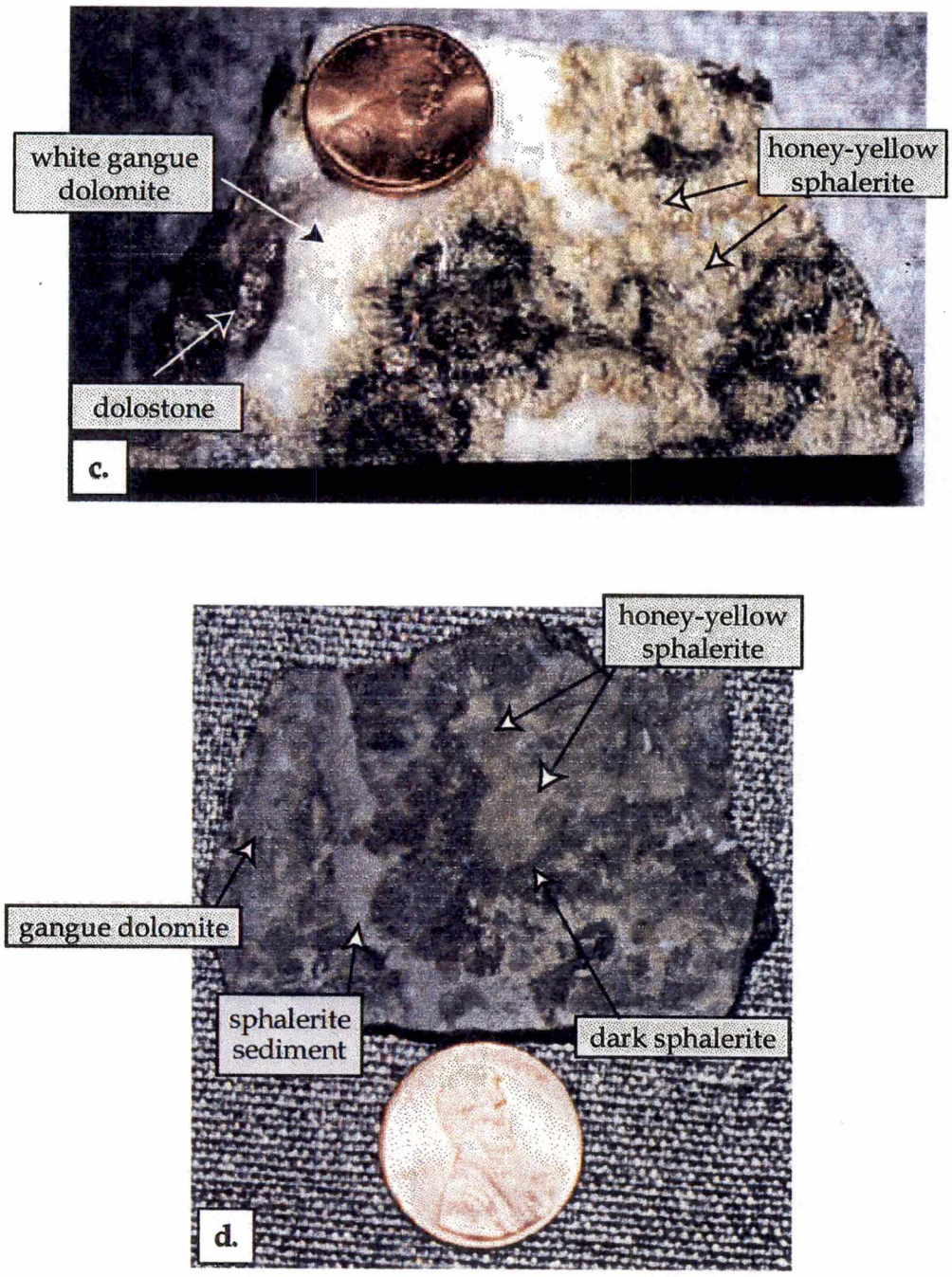

Figure 5 continued.

Figure 6. Photomicrographs of pyrite textures, Mascot-Jefferson City zinc district, East Tennessee. a. Reflected-light image of diagenetic pyrite, with very light $\delta^{34}S$ values, occurring in host dolostone (sample jp7, New Market mine); b. Reflected-light image of a sphalerite rosette with fine-grained, ore-stage pyrite occurring within an organic-rich zone (sample 3590, Coy mine); c. Reflected-light image (sample 3278, Jefferson City mine) of pyrite in contact with sphalerite; d. Reflected-light image of the pyrite band in Figure b. Open circles represent spots of SIMS analysis with corresponding $\delta^{34}S$ values (‰ CDT) noted to the side.

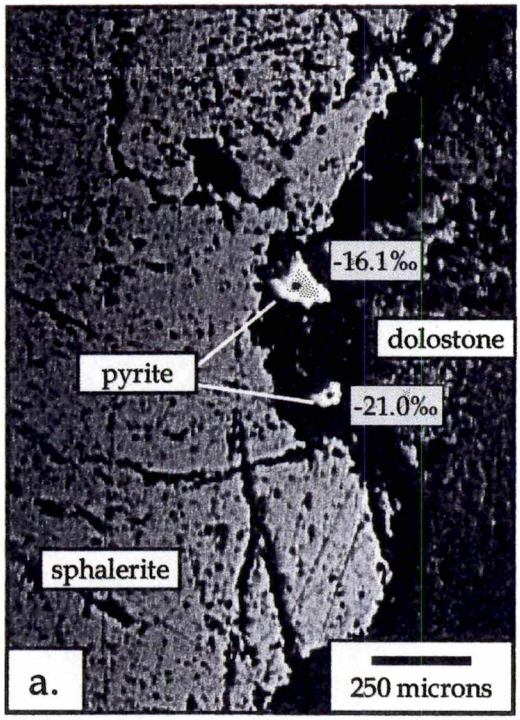
-16.1‰
dolostone
pyrite
-21.0‰
sphalerite
a.
250 microns

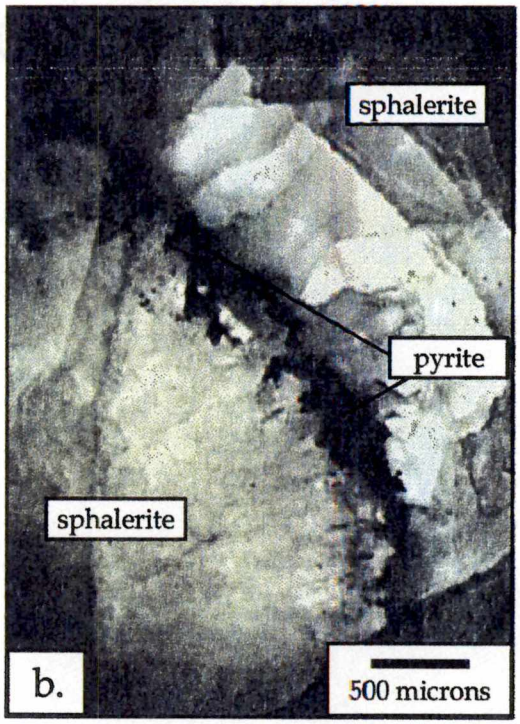
sphalerite
pyrite
sphalerite
b.
500 microns

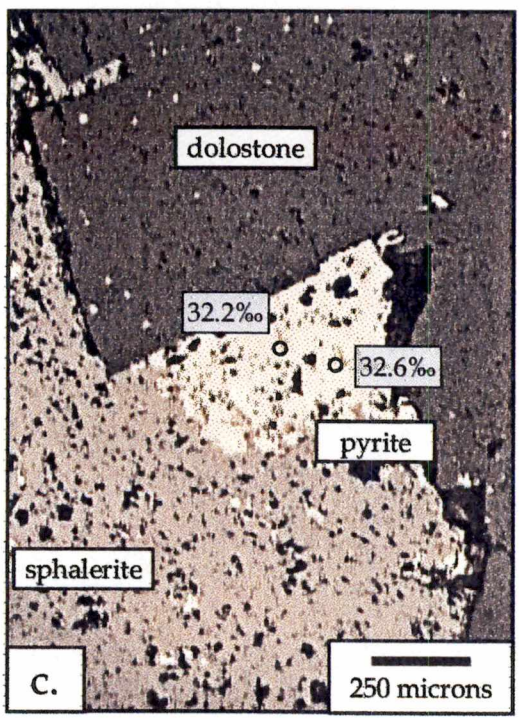
dolostone
32.2‰
32.6‰
pyrite
sphalerite
c.
250 microns

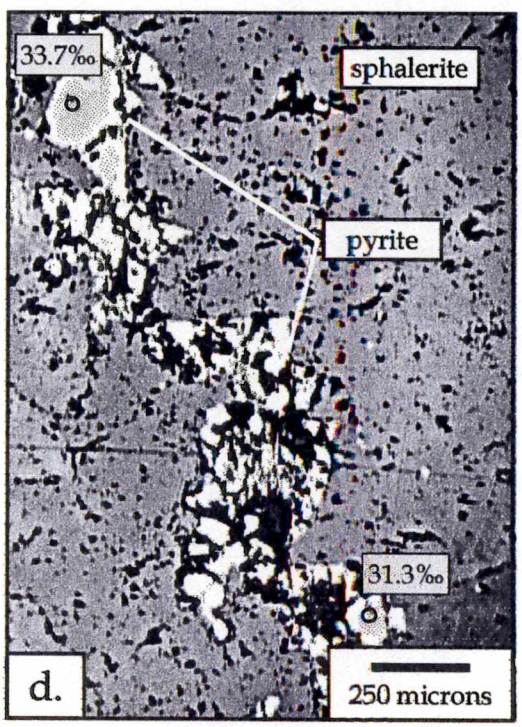
33.7‰
sphalerite
pyrite
31.3‰
d.
250 microns

associated with sphalerite as an integral component of the breccia-fill mineralization (Figures 6b,c,d), indicating pyrite precipitation broadly contemporaneous with sphalerite deposition.

The ore-gangue paragenesis is relatively simple (McCormick et al., 1971; Caless, 1983). In essence, the paragenesis encompasses 3 stages of sphalerite precipitation interspersed with multiple stages of white gangue dolomite. Subordinate amounts of pyrite and/or marcasite occur with pre-ore and main-stage mineralization (Figure 7).

Sphalerite Composition

A summary of the electron microprobe analyses of sphalerite is given in Table 1 and complete results are given in Appendix C. In general, the sphalerite has low concentrations of Fe (up to 0.4 wt. %) and Cd (up to 0.96 wt. %), although one sample from the Jefferson City mine (3272) has Fe contents as high as 7.63 wt. % with Cd less than 0.37 wt. %. The Cu concentration in the studied samples is either below the detection limit or very low (up to 0.19 wt. %). Mn was not detected in any of the sphalerite analyzed. The zoned and unzoned sphalerite have similar Fe and Cd contents, with the exception of the high-Fe sample from Jefferson City (unzoned).

Previous studies (e.g. Churnet and Misra, 1983; Craig et al., 1983) have reported similar Fe and Cd contents in sphalerite from the MJC district. In these studies, Fe content is variable but generally low (up to 1.6 wt. %) with an average

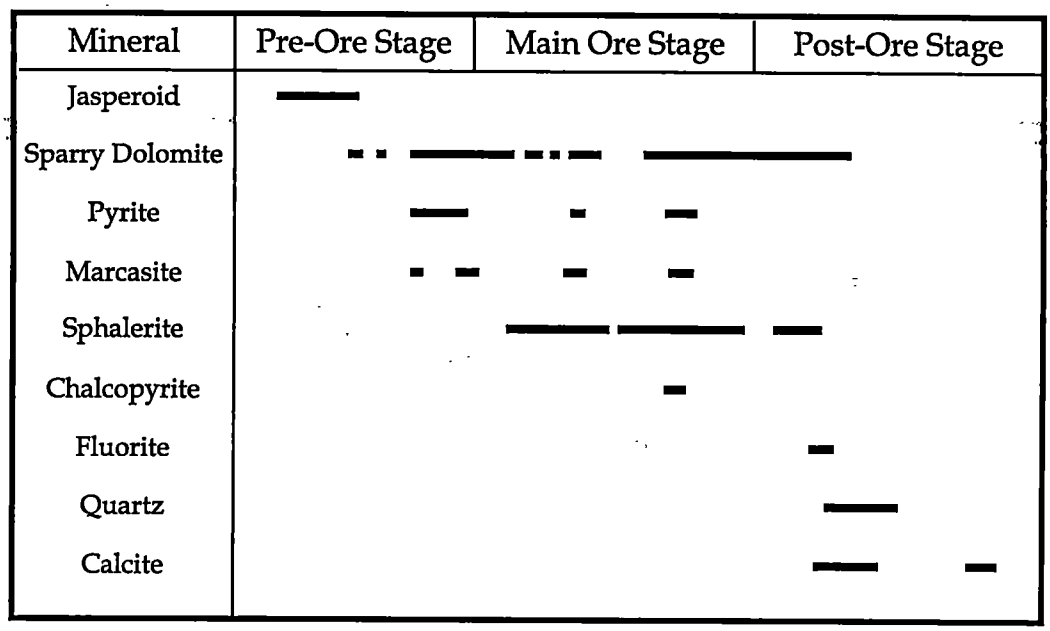

Figure 7. Paragenesis of east Tennessee zinc deposits (after Caless, 1983).

Table 1. Electron microprobe and SIMS analyses of sphalerite samples from selected mines of East Tennessee

	Jefferson City Mine				Coy Mine		New Market Mine						Young Mine	
sample	3272		3278		3590		jp2		jp5		jp7		sds1	
texture	unzoned		color zoned		rosette		unzoned		unzoned		unzoned		rosette	
	range	average	range	average	range	average	range	average	range	average	range	average	range	average
Weight Percent														
n*	[26]		[15]		[18]		[37]		[26]		[21]		[29]	
S	32.2 - 33.6	32.7	31.8 - 33.0	32.5	32.0 - 32.8	32.4	30.8 - 33.2	32.4	31.8 - 33.0	32.3	31.9 - 33.2	32.4	31.7 - 32.9	32.4
Fe	0.20 - 7.63	2.45	0.07 - 038	0.22	0.03 - 0.24	0.14	0.02 - 0.29	0.14	0.04 - 0.24	0.10	0.06 - 0.40	0.14	0.03 - 032	0.11
Zn	58.3 - 66.6	64.0	64.6 - 67.5	66.7	65.6 - 67.0	66.4	65.3 - 67.0	66.0	65.4 - 66.5	66.1	65.5 - 67.1	66.3	65.5 - 67.1	66.5
Cu	0.00 - 0.03	0.08	0.03 - 0.19	0.09	0.00 - 0.11	0.06	0.00 - 0.08	0.02	0.00 - 0.08	0.03	0.00 - 0.07	0.02	0.03 - 0.15	0.08
Cd	0.00 - 0.37	0.15	0.10 - 0.86	0.34	0.03 - 0.42	0.26	0.11 - 0.67	0.36	0.14 - 0.75	0.41	0.06 - 0.54	0.37	0.10 - 0.96	0.46
Mole Percent														
S	49.5 - 50.6	49.9	49.1 - 50.0	49.7	49.2 - 50.1	49.8	48.8 - 50.7	49.9	49.3 - 50.4	49.8	49.3 - 50.4	49.7	49.3 - 50.1	49.6
Fe	0.21 - 6.65	2.14	0.06 - 0.33	0.19	0.03 - 0.31	0.14	0.02 - 0.26	0.12	0.03 - 0.22	0.08	0.05 - 0.36	0.13	0.03 - 0.28	0.10
Zn	43.3 - 50.0	47.8	48.9 - 50.6	49.9	49.7 - 50.6	50.0	49.2 - 50.8	49.8	49.3 - 50.3	49.9	49.3 - 50.3	49.9	49.3 - 50.4	50.0
Cu	0.00 - 0.23	0.06	0.00 - 0.15	0.08	0.00 - 0.05	0.05	0.00 - 0.06	0.02	0.00 - 0.06	0.02	0.00 - 0.06	0.02	0.00 - 0.11	0.07
Cd	0.00 - 0.16	0.07	0.04 - 0.38	0.16	0.06 - 0.18	0.11	0.05 - 0.30	0.16	0.06 - 0.33	0.18	0.03 - 0.24	0.16	0.04 - 0.29	0.20
Sulfur Isotopes (‰ CDT)														
n*	[24]		[9]		[6]		[10]		[10]		[5]		[11]	
$\delta^{34}S_{sph}$	20.2 - 30.6	24.6	27.8 - 43.8	35.8	32.0 - 36.5	34.3	27.8 - 34.8	32.1	26.5 - 39.5	32.3	29.7 - 33.4	31.8	34.4 - 51.0	42.7
n*	[1]		[2]		[2]						[2]			
$\delta^{34}S_{py}$	18.8	-	32.2 - 32.6	-	31.3 - 33.7	-	-	-	-	-	-16.1 - -20	-	-	-

*n = the number of analyses included in the range and average. sph = sphalerite, py = pyrite

of less than 0.5 wt. % (Craig et al., 1983), which agrees with the findings of Churnet and Misra (1983). Cd content is similarly variable and may be as high as 3 wt. % (Churnet and Misra, 1983; Craig et al., 1983). A lack of correlation of color bands with Fe or Cd composition has been noted by several authors (e.g. Roedder and Dwornik, 1968; Foley et al., 1980). Both Churnet and Misra (1983) and Craig et al. (1983) have noted a crude correlation of dark black bands with higher Cd concentrations.

A traverse across each thin section was performed to assess compositional variations, especially among the zones in color-banded sphalerite. The traverse across growth-banded samples showed no systematic trends in chemical composition. Despite significant variations in Fe and Cd contents among color bands, the light and dark bands do not correlate with Fe and Cd content in a systematic manner (Figures 8 and 9). Unzoned sphalerite also shows variable Fe and Cd contents (Figure 10).

Backscatter electron images display relative mass differences in shades of gray. Higher mass minerals appear as lighter colors and lower mass minerals as darker colors. Cd-enriched areas are lighter gray, whereas Fe-enriched areas are a slightly darker gray and carbonate phases are black. Backscatter images do not show any difference in the zoned samples despite their variable Fe and Cd contents. Some unzoned samples show a mottled or irregular texture, which indicates continuing reaction with the sphalerite precipitating fluid. In Figure

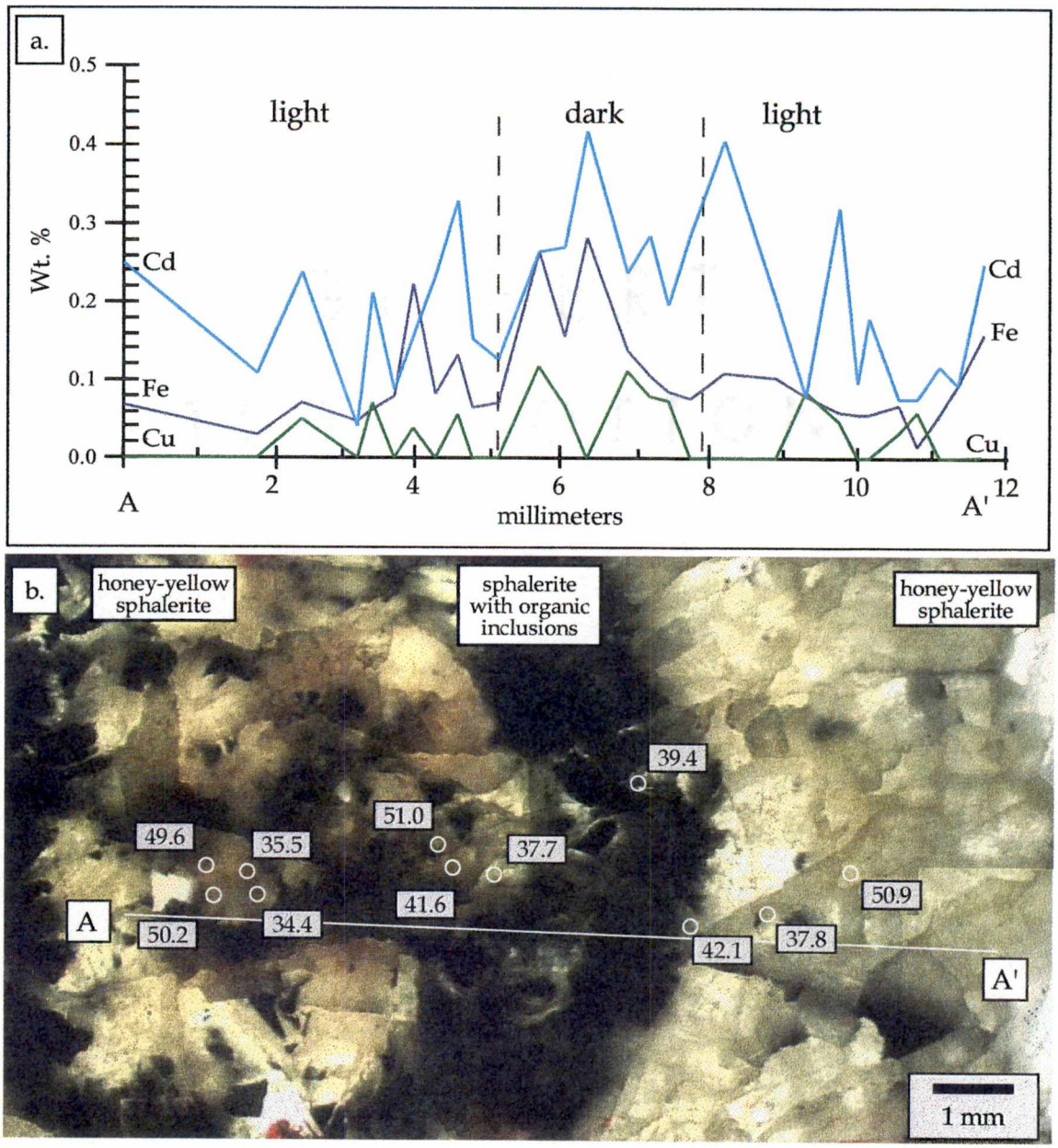

Figure 8. Sphalerite rosette (sample sds1 from Young mine) with compositional and isotopic data. a. Graph of electron microprobe data for Fe, Cd and Cu; b. Photograph of rosette under plane-polarized light. The line A to A′ represents the electron microprobe traverse and corresponds to the graph above. The open circles represent spots where ion probe data were obtained, with $\delta^{34}S$ (‰ CDT) values noted to the side.

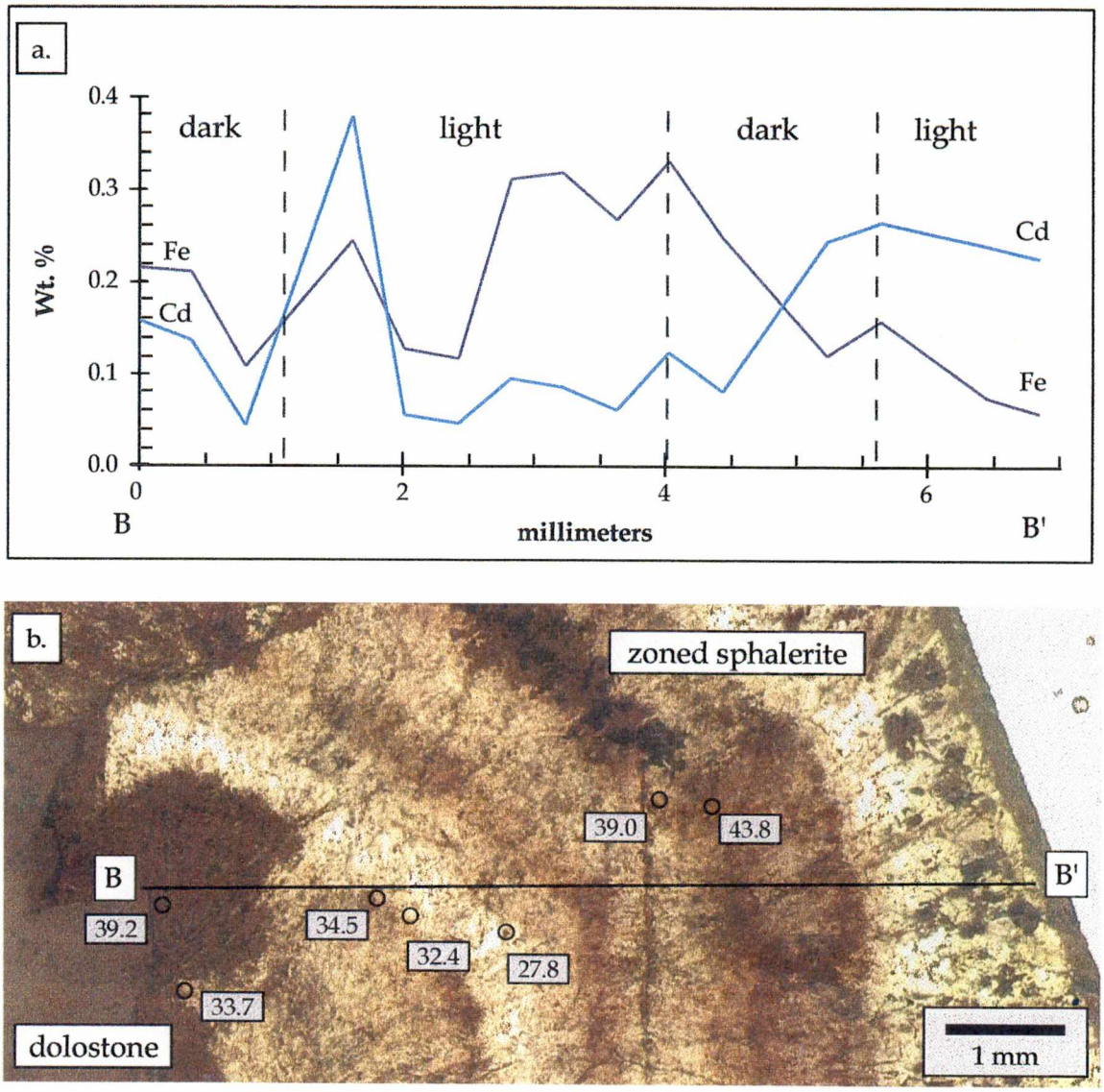

Figure 9. Growth banding in sphalerite (sample 3278, from Jefferson City Mine) with compositional and isotopic data. a. Graph of electron microprobe data for Fe and Cd; b. Photograph of sample under plane-polarized light. The line B to B' represents the electron microprobe traverse and corresponds to the graph a. above. The open circles represent spots where ion probe data were obtained, with $\delta^{34}S$ (‰ CDT) values noted on the side.

Figure 10. Unzoned sphalerite (sample jp5 from New Market mine) with compositional and isotopic data. a. Graph of point-by-point analyses of $\delta^{34}S$ and Fe and Cd contents; b. Reflected-light photomicrograph of the sample. Open circles represent spots where ion probe and electron microprobe analyses were obtained, with values noted on the graphs above; c. Backscatter electron image of the small square marked on Figure b. The darker splotches are more Cd-rich, whereas the lighter areas are more Fe-rich. Open circles represent spots where ion probe analyses were obtained, with values (‰ CDT) noted to the side.

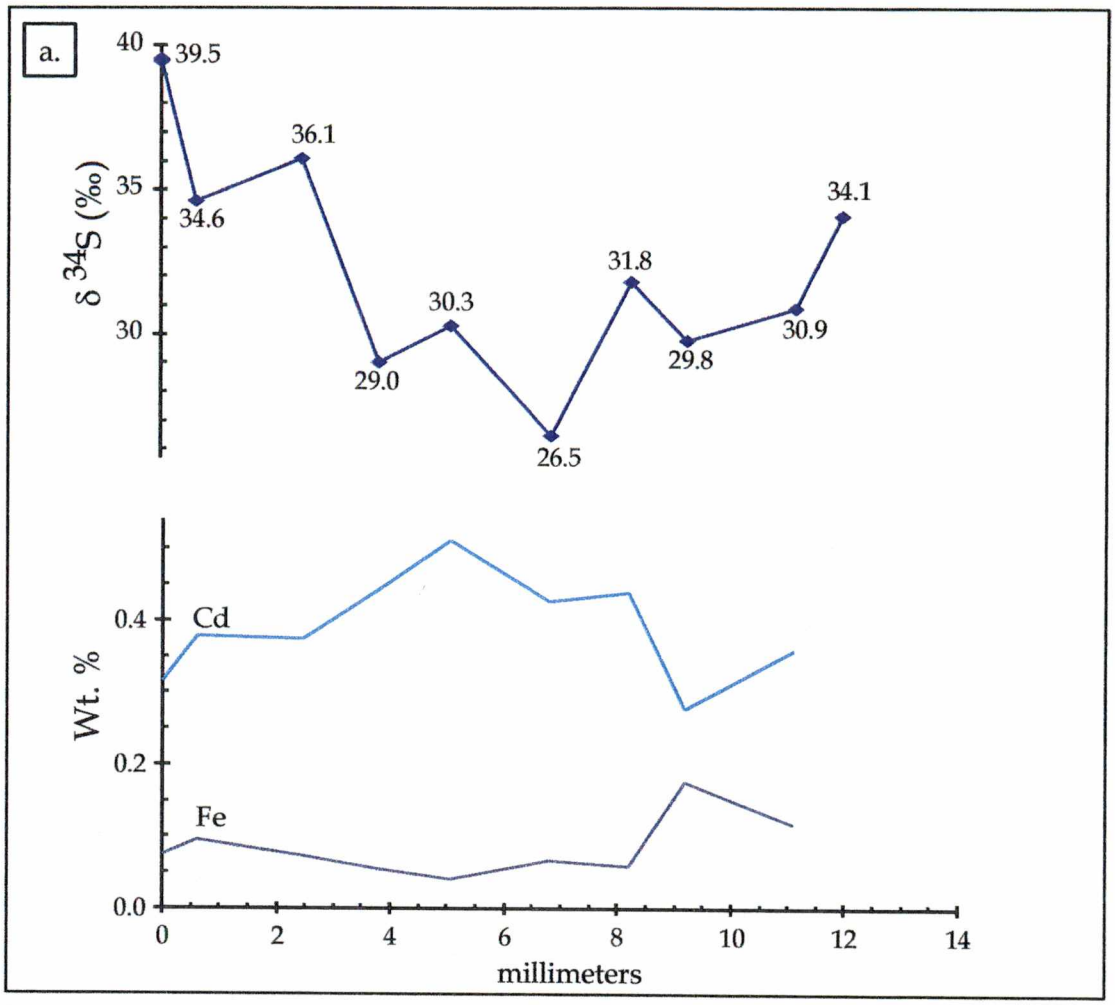
a.
40
35
30
δ 34S (‰)
39.5
34.6
36.1
29.0
30.3
26.5
31.8
29.8
30.9
34.1
0.4
0.2
0.0
Wt. %
Cd
Fe
0
2
4
6
8
10
12
14
millimeters

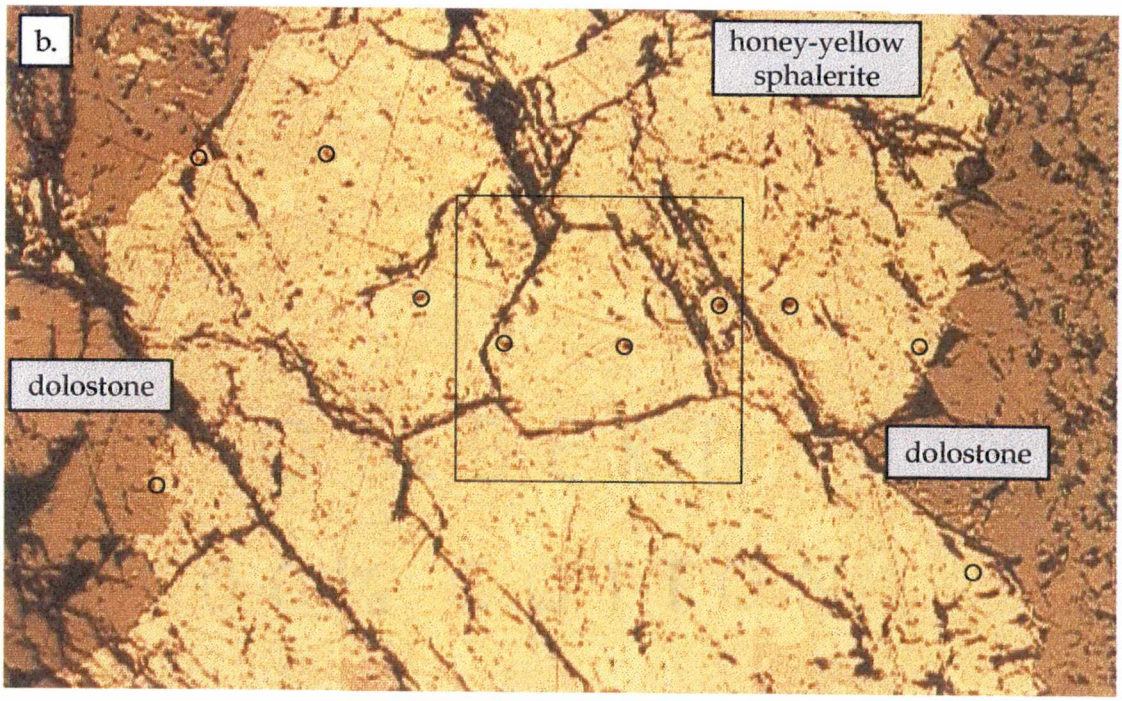
b.
honey-yellow sphalerite
dolostone
dolostone

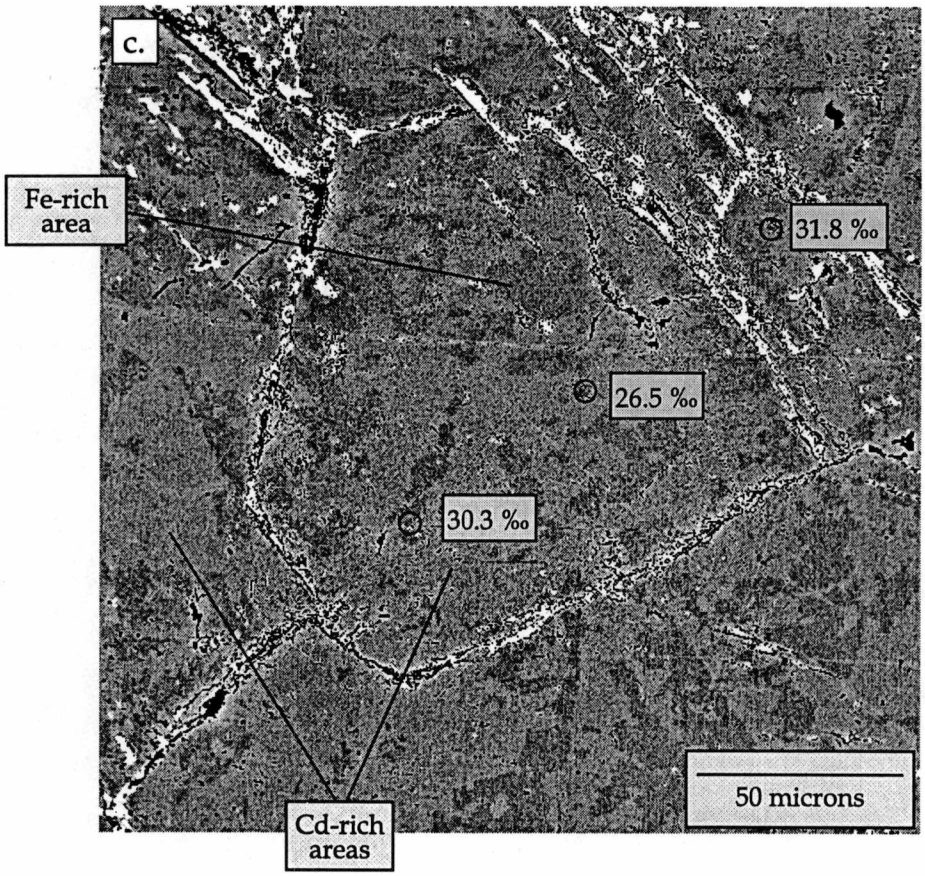
c.
Fe-rich area
31.8 ‰
26.5 ‰
30.3 ‰
50 microns
Cd-rich areas

10c, backscatter shows some splotches of differing composition within a single crystal. In this case, the Fe-enriched area corresponds to a lower $\delta^{34}S$ than the Cd-enriched area (26.5‰ and 30.3‰, respectively). Figure 11 is an example of a sample that shows very small changes in the $\delta^{34}S$ values across sphalerite that is fairly homogenous; the sphalerite also shows very little mottling under backscatter imaging.

Sulfur Isotope Ratios

Sulfur isotope analyses were performed on seven samples. Analyses were taken along a traverse across each section in order to observe variations among the different growth zones of sphalerite. The traverses corresponded with those taken during electron microprobe analyses. The results are summarized in Table 1 and Figure 12; a complete listing of analyses is given in Appendix D. $\delta^{34}S$ values for the Mascot-Jefferson City district sphalerite range from a low of 20.2‰ to a high of 51.0‰, with an arithmetic mean of 30.4‰ and a median of 29.0‰. The error in these analyses is ± 0.8‰ (1σ). Some samples (e.g. jp5, New Market mine and 3272, Jefferson City mine) showed a wide variation (as much as 15‰); however, others (e.g. jp7, New Market mine) show much smaller variation (~4‰)(Figure 12). The $\delta^{34}S$ values measured in this study span a much larger range compared with the range (27.0‰ to 36.1‰) reported by Jones (1993), and include some of the highest $\delta^{34}S$ values ever reported for MVT deposits in East Tennessee and elsewhere (Misra, 2001).

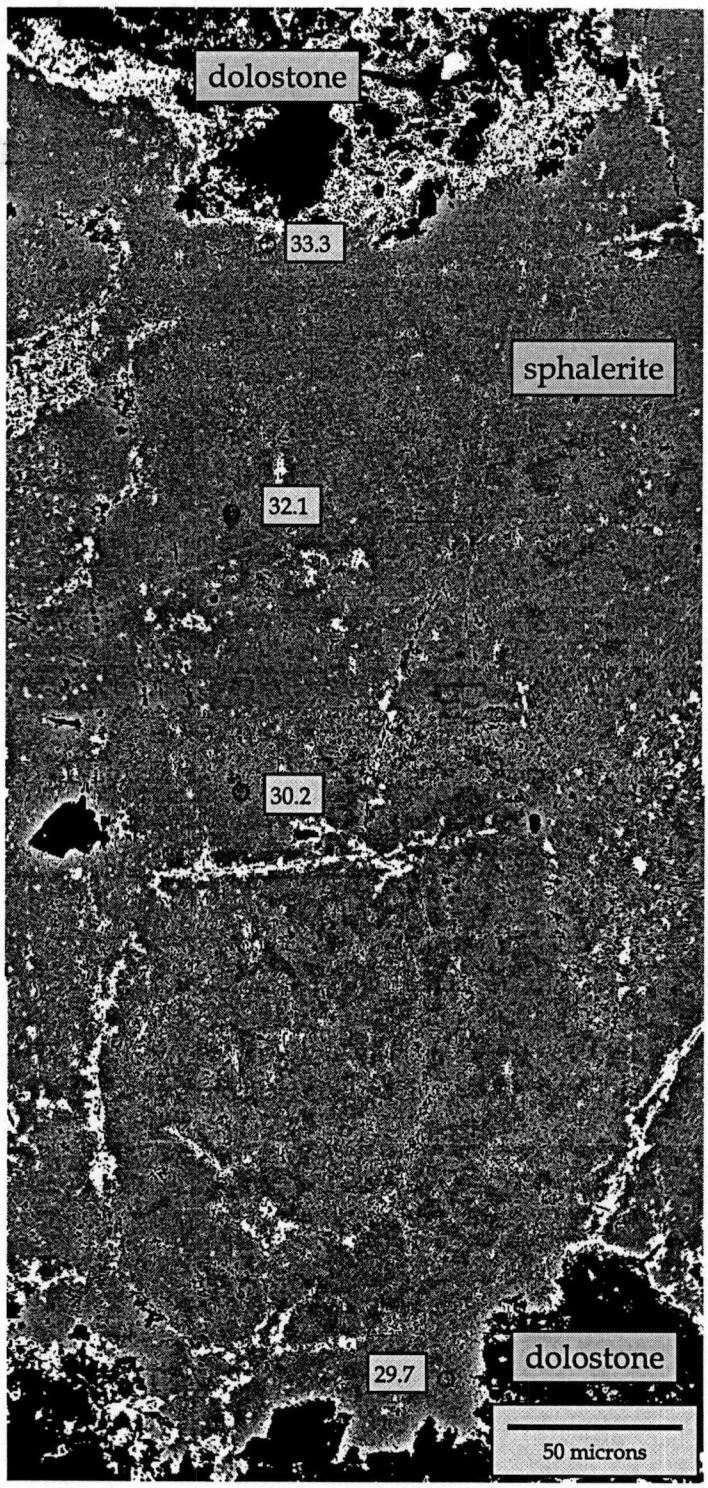

Figure 11. Backscatter image of unzoned sphalerite (sample jp7, New Market mine) with sulfur isotope values. The black areas at the top and bottom are dolomite and the gray area is sphalerite. Open circles represent spots where SIMS analyses were obtained, with $\delta^{34}S$ (‰ CDT) noted on the side. The sulfur isotope values show no significant variation across the sample.

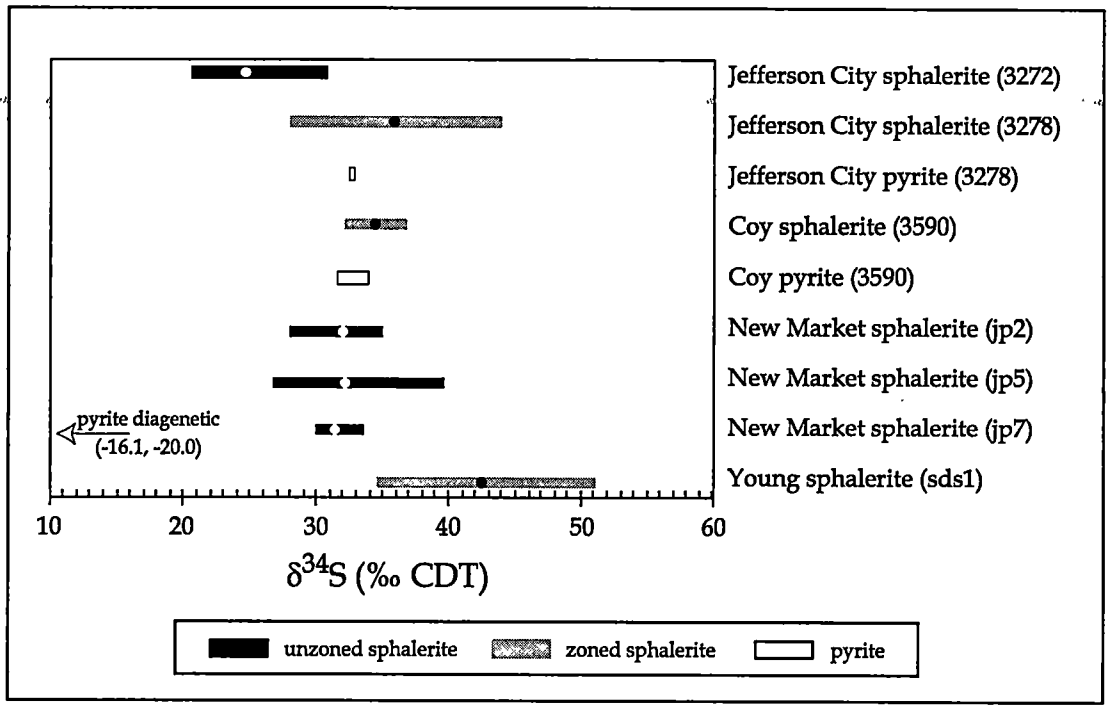

Figure 12. $\delta^{34}S$ values of pyrite and unzoned and zoned sphalerite from the Mascot-Jefferson City zinc district, East Tennessee. Mines are listed from east (top) to west (bottom). Circles represent the average of the sphalerite analyses from each mine.

There is no systematic difference between light and dark colored sphalerite in terms of chemical composition and sulfur isotope ratios, but the zoned and unzoned sphalerites appear to fall into two separate populations. The unzoned sphalerite is characterized by lower $\delta^{34}S$ values (20.2‰ to 39.5‰) and the lower Cd contents (0.00 to 0.37). In contrast, zoned sphalerite has the higher $\delta^{34}S$ values (27.8‰ to 51.0 ‰) and highest Cd contents (0.03 to 0.96 wt. %) (Table 1, Figure 12). The Fe content does not vary much between the zoned and unzoned sphalerite with the exception of one unzoned Fe-rich sample from the Jefferson City mine. The zoned sphalerite also has more organic inclusions than the relatively clean unzoned sphalerite. The lack of organic inclusions in the unzoned sphalerite may reflect a period of uniformity in the composition of the depositional fluids (Craig et al., 1983).

Sulfur isotope data on pyrite is limited because of the paucity of pyrite in the samples examined for this study, but they strongly support the interpretation of two very different generations of pyrite based on textural evidence. The pre-sphalerite, diagenetic pyrite has a very different isotopic signature (–16.1‰ and –20.0‰) compared with the syn-sphalerite pyrite (33.7‰ to 31.3‰), which is intergrown with sphalerite of similar isotopic signature (32.0‰ to 39.2‰)

Sulfur isotope data from coexisting sphalerite and pyrite were used for geothermometry. Using the geothermometer of Ohmoto and Rye (1979), one pair of pyrite-sphalerite data yielded a temperature of 149° ± 31°C, which is in

good agreement with fluid inclusion homogenization temperatures determined in this study as well as by earlier workers (e.g. Roedder, 1971; Taylor et al. 1983). Another pair was unusable apparently due to isotopic disequilibrium between the sulfides. Based on the bond energy consideration, Bachinski (1969) noted that pyrite should be more enriched in ^{34}S relative to sphalerite when the two minerals are in equilibrium. Since the pyrite (~ 32‰) in this pair has a lower $\delta^{34}S$ signature than the coexisting sphalerite (39.2‰), the two minerals in this case are not in isotopic equilibrium and probably represent non-contemporaneous deposition at different temperatures.

Fluid Inclusion Microthermometry

Paired homogenization and freezing temperatures were obtained from six specimens. Sphalerite is notoriously hard to work with (e.g. Roedder, 1971), and often inclusions were too small or hard to find. This problem makes it difficult to correlate the homogenization temperature to $\delta^{34}S$ values or chemical composition. A complete listing of fluid inclusion microthermometric measurements is given in Appendix E. The homogenization temperature for 48 observations ranged from 85.6 to 194.5°C with an average of 139.2°C, and the freezing temperature (temperature of last ice melting) ranged from –39.8 to –7.3°C with an average of –21.8°C (Figure 13).

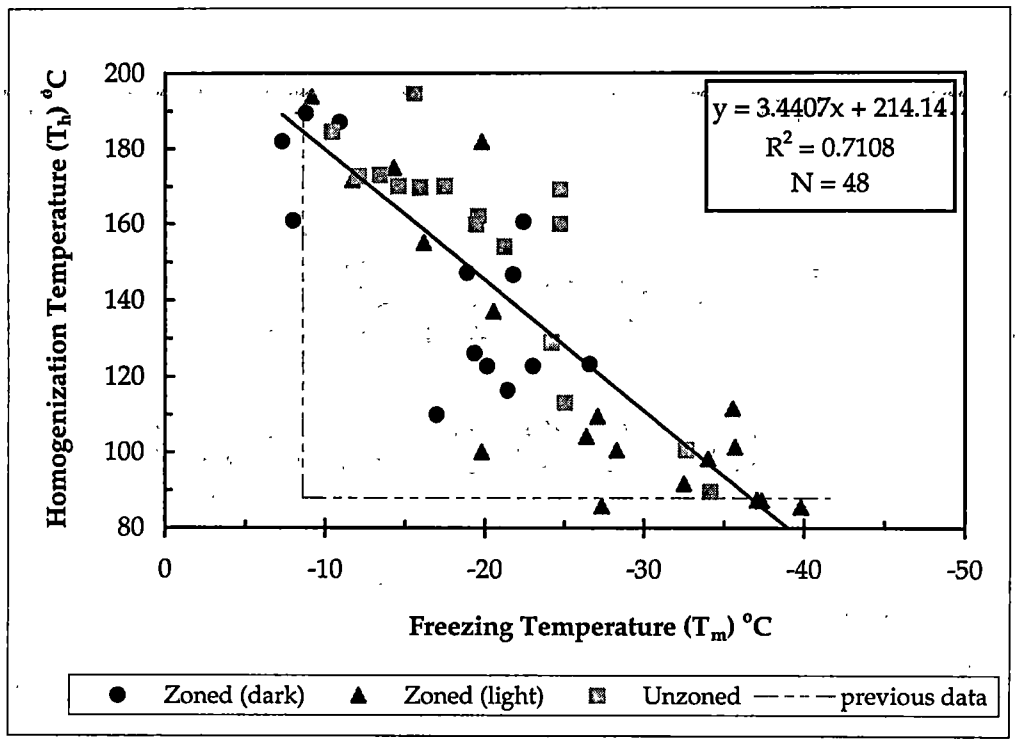

Figure 13. Paired freezing temperature and homogenization temperature data for primary fluid inclusions in sphalerite samples from the Mascot-Jefferson City zinc district, East Tennessee. The "previous data" heading refers to the range of homogenization and freezing temperatures reported by Taylor et al. (1983).

Earlier microthermometric analyses of fluid inclusions in Mascot-Jefferson City sphalerites (Roedder, 1971; Taylor et al., 1983) have yielded a similar range of homogenization and freezing temperatures. For example, the ranges observed in the detailed fluid inclusion studies by Taylor et al. (1983) are 88° to 197°C and -8.6° to -41.6°C, respectively. However, the local scale variations are much smaller. They noted a variation of about 15°C in the homogenization temperature and 3°C in the freezing temperature between the core and rim of a sphalerite rosette (Figure 14).

There is an overall inverse correlation between homogenization temperature and freezing temperature. Attempts were made to correlate the homogenization temperature with color bands. The data suggest that there may be a correlation between zoned dark sphalerite with higher homogenization temperatures and zoned light sphalerite with lower homogenization temperatures. This relationship is not systematic, possibly due to the smaller number of analyses and uncertainty associated with distinguishing light bands from dark bands during the analyses. Unzoned sphalerite has homogenization temperatures that span the entire range of observations.

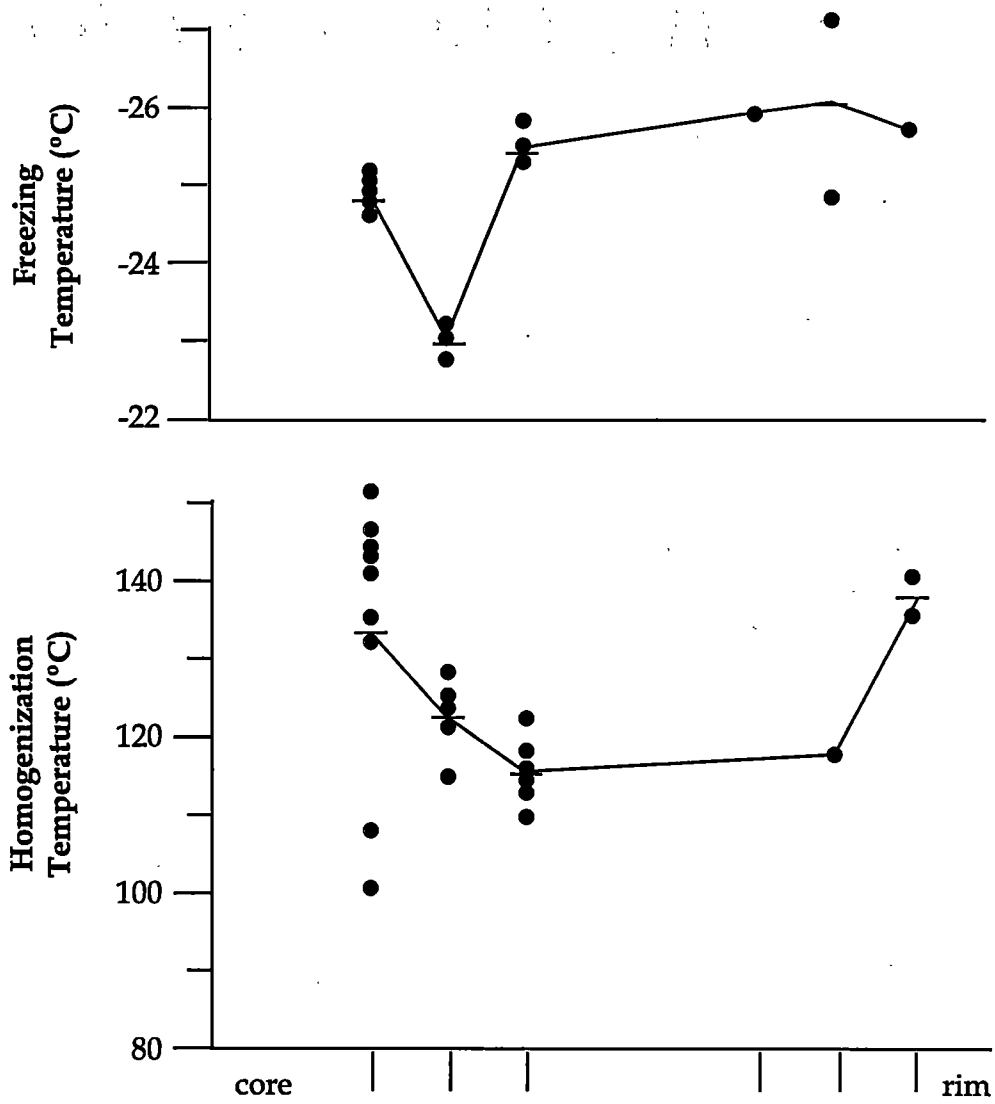

Figure 14. Variations in homogenization and freezing temperatures in a sphalerite rosette from core to rim. Horizontal lines represent the average of the data points. Data from Taylor et al. (1983).

Chapter Five

Interpretation and Discussion

Analyses of the sphalerite from the Mascot-Jefferson City district indicate that sphalerite is generally low in Fe (up to 0.4 wt. %) and also low in Cd (up to 0.96 wt. %). The samples show a wide range of $\delta^{34}S$ values (20.2‰ to 51.0‰) with an average of 31.8‰ for all analyses (Table 1). The $\delta^{34}S$ variation within a single sample is small in some thin sections (~4‰) and quite large in others (up to 15‰)(Table 1). The $\delta^{34}S$ range obtained in this study (20.2‰ to 51.0‰) is comparable to that reported by Jones (1993) for bulk sulfides (27.0‰ to 36.1‰, with 80% > 30‰), although the present data span a wider range and includes some of the highest values ever reported for MVT deposits.

The two textural types of sphalerite examined in this study - unzoned sphalerite, and color banded or zoned sphalerite - appear to be somewhat distinct in terms of chemical and isotopic composition. The zoned sphalerite has the heaviest $\delta^{34}S$ values (27.8‰ to 51.0‰), low Fe contents (0.03 to 0.32 wt. %), and the highest Cd contents (0.03 to 0.96 wt. %) (Table 1, Figure 12).

This study found no obvious and systematic correlation between color banding and chemical composition (Figures 8 and 9). The lack of correlation between composition and color of sphalerite was also noted in previous studies by Caless (1983) and Churnet and Misra (1983). The dark color bands have been attributed a higher concentration of minute organic carbon inclusions (Craig et

al., 1983; Kettler, 1990). In this study, darker bands corresponded to the some of the highest Cd contents noted within the samples (Figure 8) as was also noted by Craig et al. (1983). The dark bands tend to show higher $\delta^{34}S$ values in one sample (Figure 9). In another sample, the dark band has mid-range values (37‰ to 42‰)(Figure 8), whereas the highest values occur in both light and dark areas. The data collected in this study are not enough to establish a distinct correlation between dark bands and high $\delta^{34}S$ values. There is, however, a crude correlation between Fe content, Cd content, and $\delta^{34}S$. Samples with higher Fe contents tend to have lower $\delta^{34}S$ values (20.2‰ to 39.4‰), whereas samples with lower Fe contents and higher Cd contents tend to have higher $\delta^{34}S$ values (32.0‰ to 51.0‰)(Figure 15), a trend particularly discernable at the highest (Young mine) and lowest (Jefferson City mine) ends of the $\delta^{34}S$ spectrum. The zoned sphalerite samples also have more organic inclusions than the relatively clean, unzoned sphalerite. The presence of organic inclusions in zoned sphalerite reflects a period of high organic input and is possibly related to the sulfur source or reduction mechanism.

There seems to be a geographic trend in the data such that the eastern-most mine (Jefferson City, Figure 4b) has the lowest $\delta^{34}S$ values and highest Fe contents and the western most mine (Young Mine) has the highest $\delta^{34}S$ values and highest Cd contents (Figure 15b and c). Data from the remaining mines clusters in the intermediate values for Fe, Cd and $\delta^{34}S$. McCormick et al. (1971)

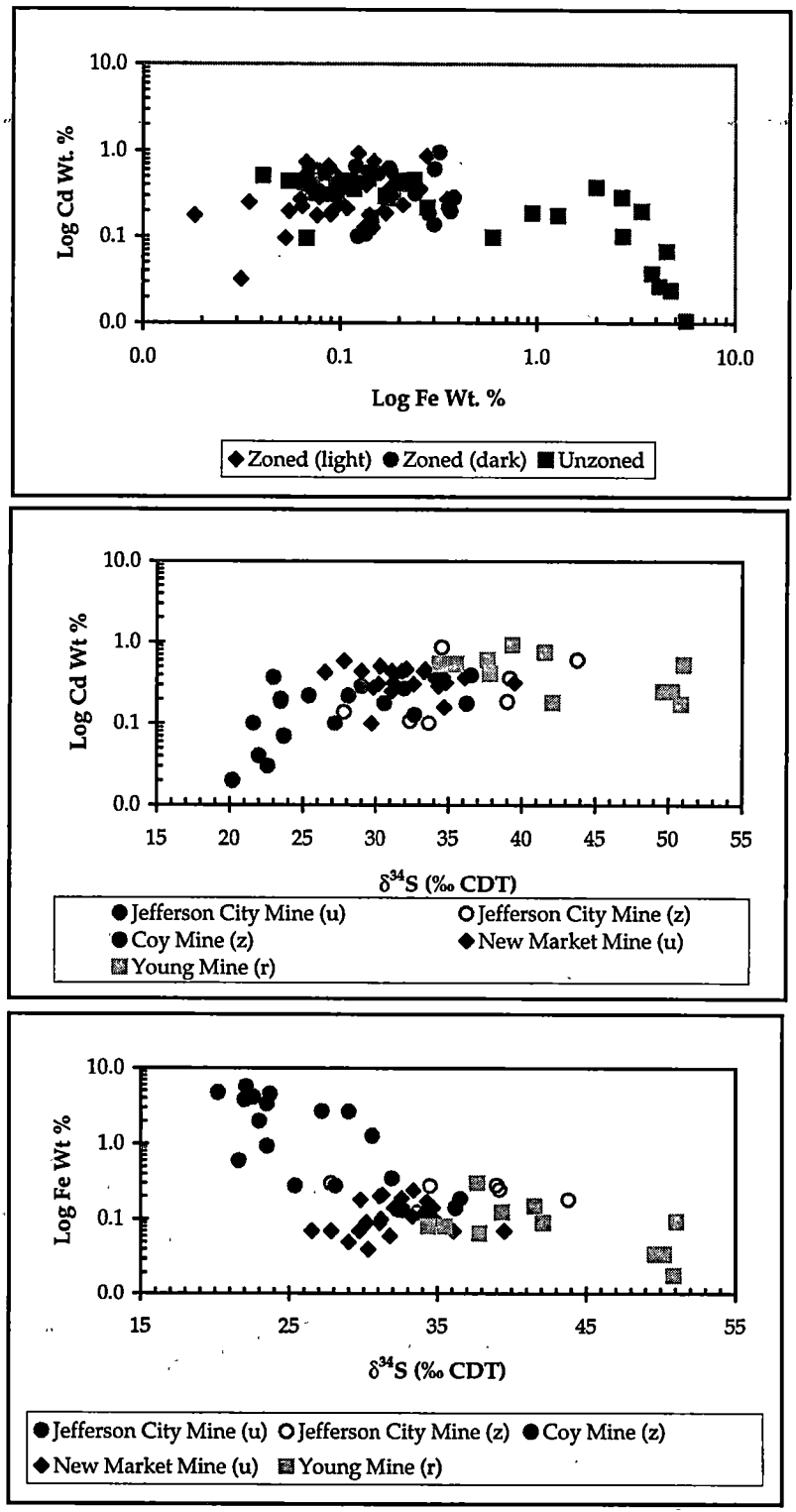

Figure 15. Relationships between Fe and Cd contents and $\delta^{34}S$ for unzoned (u), zoned (z) and rosette (r) sphalerite from the Mascot-Jefferson City zinc district, East Tennessee. The Jefferson City mine is the eastern-most mine in the district and the Young mine is the western-most mine in the study area.

noted that the depth to mineralization is not uniform across the district; the mines in the east have greater (25m) depth to mineralization than those in the west. Nakai et al. (1993) obtained sphalerite ages of 377 ± 29 Ma for the Coy mine sphalerite and 347 ± 20 Ma for the Immel mine; however, because of the large error in the data, no conclusion can be drawn from this with respect to the age of sphalerite mineralization in the two mines. Each mine has a slightly different but overlapping range of $\delta^{34}S$ values (Figure 12). This trend was also noted by Jones (1993) who attributed the differences to smaller gas pockets rather than a continuous gas cap. The differences from mine to mine might reflect continuing evolution of the fluid as it migrated along the flow path such that the fluid would become more enriched in ^{34}S and depleted in Fe leaving more distal mines with higher $\delta^{34}S$ values and less Fe.

The large variation in $\delta^{34}S$ (~30‰) within the Mascot-Jefferson City district and the considerable microscale variations even within single samples (up to 15‰) indicate multiple mechanisms of sulfate reduction and sphalerite precipitation. To understand the complexities in the sulfur isotope data, the parameters affecting the sulfur isotope signature were examined as a preliminary approach.

Factors affecting $\delta^{34}S$ in sphalerite

Factors affecting the sulfur isotope signature of hydrothermal sulfide minerals are: temperature, pH, and fO_2 of the fluid as well as the $\delta^{34}S$ value of the

H_2S responsible for precipitating sulfides (Sakai, 1968; Ohmoto, 1972). As mentioned earlier, fluid inclusion homogenization temperatures for MJC sphalerite span a considerable range, indicating appreciable fluctuations in temperature during the history of sulfide deposition, even during the growth of a single sphalerite rosette (Figure 13 from Taylor et al., 1983). Temperature of sphalerite precipitation, however, could not have been a significant factor in producing the observed $\delta^{34}S$ variations, because sulfur isotopic fractionation between H_2S and ZnS is very small and virtually independent of temperature (Figure 16). The fractionation between sulfate and H_2S shows a strong temperature dependence, which will be discussed in a later section. Calculations presented by Ohmoto (1972) suggest that within the stability field of sphalerite, changes in pH and fO_2 would produce only very small variations in $\delta^{34}S$ (sphalerite). Thus, the variations in $\delta^{34}S$ (sphalerite) appear to have been controlled predominantly by variations in $\delta^{34}S$ (H_2S) during sphalerite deposition, and the very high positive values of $\delta^{34}S$ (sphalerite) reflect correspondingly high positive values of $\delta^{34}S$ (H_2S).

The source of H_2S for MVT sulfides is believed to be seawater sulfate either as a dissolved component of connate water or as evaporite minerals According to the secular curve presented by Claypool et al. (1980), the $\delta^{34}S$ of seawater sulfate during the upper Cambrian and lower Ordovician was about 27‰ to 32‰. Factoring in the uncertainty in the seawater sulfate curve, the

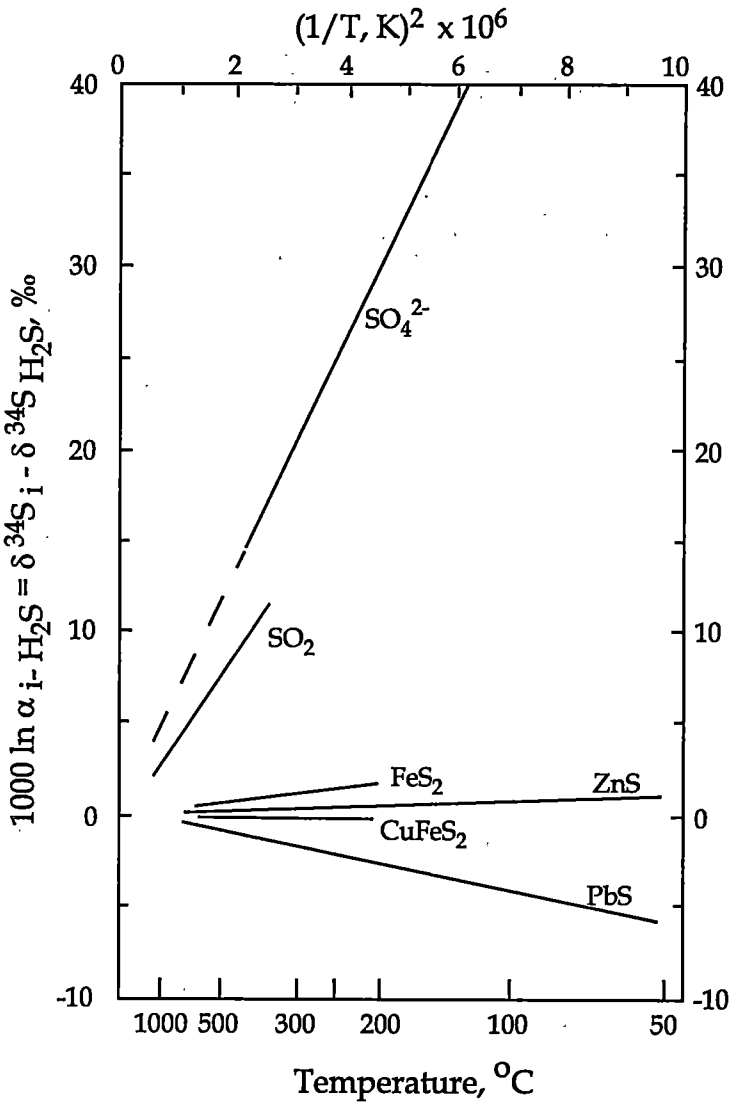

Figure 16. Fractionation curves of sulfur species relative to H_2S as a function of temperature (Ohmoto and Rye, 1979).

seawater sulfate may have been as low 26‰ or as high as 34‰; a median value of 30‰ has been assumed for the purpose of this study.

To explain how seawater sulfate produced sulfide minerals with $\delta^{34}S$ values ranging from 20-51‰, various genetic models were examined. From the perspective of sulfur isotope data, a viable genetic model for the MJC deposits must explain three basic observations: a) the large range of sphalerite $\delta^{34}S$ values, b) the considerable microscale variations in the $\delta^{34}S$ values; and c) some unusually high positive $\delta^{34}S$ values.

Proposed Genetic Models for MVT Deposits

Four general models have been proposed to account for the transport and deposition of base metal sulfides in MVT deposits (for reviews see Anderson and MacQueen, 1982; Sverjensky, 1981). The four models may be divided into two basic categories: mixing, and non-mixing.

Mixing

1) Base metals and reduced sulfur (dominantly H_2S at pH below 7) are transported in separate fluids to the site of deposition and mixing of the two fluids causes sulfide precipitation (Anderson, 1973, 1975, 1983, 1991; Beales, 1975).

Non-Mixing or single fluid transport

2) Base metals are transported as organic complexes in neutral to alkaline solutions and sulfide deposition results from oxidation or

pH decrease (Giordano and Barnes, 1979; Barnes, 1983; Gize and Barnes, 1987).

3) Base metals and reduced sulfur are transported in the same fluid at low pH, and precipitation is caused by an increase in pH, cooling, or a reduction in salinity due to dilution (Helgeson, 1970; Anderson, 1973; Sverjensky, 1981).

4) Base metals and oxidized sulfur (SO_4^{2-}) are transported by the same fluid to the site of deposition where the oxidized sulfur is reduced to H_2S by organic matter or sulfides causing the precipitation of sulfides (Barton, 1967; Olson, 1984; Garven, 1985).

Each of these models was examined to determine which would provide the best explanation for observed $\delta^{34}S$ data.

The mixing model advocated by many authors for MVT deposits (Taylor et al., 1983; Zimmerman et al., 1981; Foley et al., 1981; Kessen et al., 1981; Sasaki and Krouse, 1969; Cumming and Robertson, 1969; Anderson, 1973, 1975, 1983, 1991) invokes two different fluids for the precipitation of sulfides. One fluid carries the dissolved metal while the other provides reduced sulfur. Precipitation occurs when the two fluids meet and mix. The problems with this mechanism include ore body size limitations, textural evidence and isotopic evidence. Hydrologic models predict much smaller ore bodies at the mixing front rather than the large continuous ore bodies observed in most MVT districts

(Garven, 1985). Ebers and Kopp (1979) noted cathodoluminescence zones in white gangue dolomite that were could be correlated over large distances (~100's km), which is inconsistent with mixing. Craig et al. (1983) noted similarity in sphalerite growth bands from different locations (~300 meters apart in lateral distance) from East Tennessee and suggested that such correlation was inconsistent with a mixing model. Consistency of lead and sulfur isotope ratios, mainly from the Viburnum Trend in Southeast Missouri, is also compatible with a single fluid model (Sverjensky, 1981; Crocetti and Holland, 1989).

These arguments can be countered to a large extent by the presence of a stationary gas cap that contributes reduced sulfur to react with a migrating metal-bearing brine (e.g., Jones, 1993). Jones and Kesler (1992) found CH_4 (up to 3 mol. %) and H_2S (100 - 250 ppm molar) in primary fluid inclusions in sphalerite from the Mascot Jefferson City district suggesting the former presence of a gas cap. Mass balance calculations indicated that a gas cap would have to be roughly as large as the Mascot-Jefferson City zinc district to produce the amount of ore present in the district. The gas cap invoked need not be a single continuous body but rather multiple gas pockets may account for variability in $\delta^{34}S$ (sphalerite) noted between mines noted both in Jones (1993) and in the present study (Figure 12). The gas cap acted as a finite reservoir of sulfur, and caused the precipitation of sphalerite when the migrating fluid encountered the gas cap (Jones, 1993). H_2S provided solely by the gas cap in the presence of

result in rapid precipitation of sphalerite with a very fine-grained texture, which is not the most common texture of sphalerite in the MJC district.

Sulfur and metals (Pb, Zn) may be carried in organic metal sulfide complexes to the depositional site (Giordano, 1981). This mechanism has the potential to explain the transport of ore constituents; however, the specific ligands have not been identified, and known stable organic complexes in hydrothermal fluids are incapable of carrying the amount of metal and sulfur required to form a sizeable ore deposit (Giordano and Barnes, 1979). Additionally, known organic acids are generally not abundant enough to account for ore deposit scale mineralization (Kharaka et al., 1986; Gize and Barnes, 1987).

Several authors (e.g., Sverjensky, 1981, 1984; Helgeson, 1970) have argued for a single-fluid transport of metals and H_2S at a relatively low pH to explain the precipitation of sulfides in MVT deposits. Based on CO_2 contents and temperatures of fluid inclusions, Haynes et al. (1989) suggested that for East Tennessee zinc deposits, both reduced sulfur and metal were transported in a single fluid of low pH (~4). Sphalerite precipitation occurred when the pH of the fluid increased or the temperature decreased (due to reduced pressure) although they did not provide any explanation for the origin of acidic fluids. Jones and Kesler (1992) have argued that the CO_2 contents of Haynes et al. (1989) were overestimated by at least a factor of two. Also, Jones (1993) noted a lack of

feldspar indicating a pH greater than 5.5. In any case, the mechanism seems improbable for the MJC district, where the mineralizing fluid would have to maintain a low pH, in spite of traveling a considerable distance through carbonate rocks.

Metals may be transported in the same fluid along with SO_4^{2-}, which is then reduced at the depositional site to precipitate sulfides. This mechanism is the most probable and circumvents the constraint of unrealistically low pH in the single fluid model and the requirement of a fairly extensive source of reduced sulfate at the depositional site in the fluid-mixing model. This model requires the presence of a reductant at the site of precipitation. The reductant could be sulfate reducing bacteria, solid organic bitumen, petroleum sulfur or methane from a gas cap. Each of these reductants were examined in an effort to further support the proposed model.

Mechanism of Sulfate Reduction

Bacterial reduction of sulfate is the most efficient means for causing a large fractionation between H_2S and SO_4^{2-} at low temperatures. If the system remains closed to SO_4^{2-} but open to H_2S, precipitation of ^{32}S-enriched sulfides would drive the composition of the remaining sulfate to very high (^{34}S-enriched) values. This effect may be as much as 40‰ (Ohmoto, 1986). However, the upper temperature limit of BSR is about 80°C, above which almost all sulfate reducing bacteria (e.g. *Desulfovibro desulfuricans*) cease to metabolize (Machel, 1989). Thus

it is unlikely that BSR plays a major role in sediments buried to depths of more than 2000-2500 meters at near-normal geothermal gradients (Machel et al., 1995). During the late Ordovician, the shales of the Sevier basin were buried 5 to 6 km at temperatures about 200°C (Walker and Foreman, 1990).

Thermal maturation of sulfur-bearing organic compounds produces CH_4 along with H_2S. Both gases have been found in fluid inclusions from the MJC district (Jones and Kesler, 1992). H_2S is produced by reactions such as (Leventhal, 1990).

$$HR_aCH_2\text{-}S\text{-}H \rightarrow R_bCH_2 + H_2S \qquad (1)$$

where R_x represents a large organic molecule. However, as discussed by Anderson (1991) and Machel et al. (1995), virtually all H_2S-rich natural gas occurrences at temperatures of about 80°C or higher are believed to have been formed by thermochemical sulfate reduction by reactions such as (Leventhal, 1990; Machel et al., 1995):

$$4R\text{-}CH_3 + 3SO_4^{2-} + 6H^+ \rightarrow 4R\text{-}COOH + 4H_2O + 3H_2S \qquad (2)$$

These H_2S occurrences are found only at depths approaching or greater than 3,000 meters, where the temperature becomes high enough to activate TSR, but TSR can also be activated at shallow depths due to the passage of hot mineralizing fluids over a sufficiently long time (Anderson, 1991).

During maturation of organic matter, organically bound sulfur may be released as H_2S gas with little or no isotopic fractionation, and later liberated by

invading hot hydrothermal fluids (Ohmoto, 1986). Such interactions with organic matter generally result in complete conversion of sulfate to sulfide in a relatively short amount of time (Ohmoto and Rye, 1979). Thus $\delta^{34}S$ of the H_2S generated by this process would be similar to the initial $\delta^{34}S$ of the sulfate. However, to account for the observed $\delta^{34}S$ (sphalerite) values, the starting $\delta^{34}S$ (sulfate) would have to be in the range of ~20‰ to as high as ~50‰. Reduction by organic matter could incorporate some organic matter in sphalerite accounting for the presence of organic carbon in zoned sphalerite.

The $\delta^{34}S$ values of H_2S associated with petroleum are on average 15‰ lighter than seawater sulfate, but about equal to the $\delta^{34}S$ of petroleum sulfur (Thode and Monster, 1973). H_2S produced by this process would result in sulfides with $\delta^{34}S$ values around 15‰ if $\delta^{34}S$ of starting sulfate were 30‰. These values are much lower than those reported here as well as those reported in Jones (1993).

Thermochemical reduction of sulfate in a system closed to sulfate (i.e., sulfate reduction proceeds at a faster rate than sulfate supply) may be a possible mechanism to explain the high $\delta^{34}S$ (sphalerite) values noted in this study. Thermochemical sulfate reduction may be an equilibrium or kinetic process depending on whether the system is open or closed. The $\delta^{34}S$ values of the H_2S, and hence the resulting sulfides, are determined by whether the system is open or closed with respect to H_2S. If the system is closed to both SO_4^{2-} and H_2S,

equilibrium may be maintained between SO_4^{2-} and H_2S during sulfate reduction (Figure 17a). The $\delta^{34}S$ value for both would increase as more and more SO_4^{2-} is reduced, with a constant difference between $\delta^{34}S$ (SO_4^{2-}) and $\delta^{34}S$ (H_2S) determined by the fractionation factor $\alpha_{SO42-H2S}$. In this case, the H_2S can only attain a maximum $\delta^{34}S$ value equal to the $\delta^{34}S$ value of the original sulfate (i.e., ~30‰) when the sulfate is completely reduced. Assuming complete sulfate reduction, this process may account for $\delta^{34}S$ (sphalerite) values that are on the order of ~30‰, but not for values near 40-50‰, which rules out equilibrium fractionation as a possible explanation for the observed $\delta^{34}S$ data.

Alternatively, the system may be closed to sulfate but open to H_2S, in the sense that H_2S is fixed instantaneously as sulfide minerals (Rayleigh fractionation). In this situation, the $\delta^{34}S$ (H_2S) would increase rapidly with increasing degree of sulfate reduction (Figure 17b). The $\delta^{34}S$ of the total H_2S ($\delta^{34}S$ Σ_{H2S}) - i.e., the bulk $\delta^{34}S$ of the accumulated sulfides - would also increase with increasing degree of sulfate reduction, reaching a maximum value equal to the $\delta^{34}S$ of the original sulfate (~30‰) when the sulfate is completely reduced. Thus, Rayleigh fractionation can explain the high $\delta^{34}S$ (sphalerite) values observed in this study. For example, as shown in Figure 17b, reduction of sulfates with $\delta^{34}S \approx$ 30‰ should be capable of producing H_2S/sulfides of $\delta^{34}S$ = 51‰ (at T = 100° and 200°C), the highest observed $\delta^{34}S$ (sphalerite), for f=0.5. At 100° C, this process should also have produced a spectrum of $\delta^{34}S$ (sphalerite) values in the range of

Figure 17. Sulfur isotopic relationships between coexisting aqueous SO_4^{2-} and H_2S for sulfate reduction in a system closed to sulfate. a. equilibrium conditions: the system is closed to both SO_4^{2-} and H_2S; b. non-equilibrium conditions (Rayleigh fractionation); the system is closed to SO_4^{2-} but open to H_2S; c) Rayleigh fractionation with stepwise decrease in temperature and corresponding α values; the arbitrarily assumed steps are 200°, 180°, 160°, 140°, 120° and 100°C at f = 1.0, 0.8, 0.6, 0.4, 0.2 and 0.0, respectively. f is the fraction remaining at time t such that at f = 1.0, SO_4^{2-} = 100% and at f = 0.0, H_2S = 100%. The α-values were calculated from the equation of Kiyosu and Krouse (1990) at a temperatures of 140°, 100° and 200°C for graphs a and b and at stepwise temperatures for graph c. The H_2S curves show instantaneous $\delta^{34}S$ values of the reduced H_2S for a given value of f, and the Σ H_2S curves show the $\delta^{34}S$ value of the total reduced H_2S accumulated up to that point. These diagrams assume an initial $\delta^{34}S$ SO_4^{2-} = 30‰, based on the seawater sulfate value for the Ordovician (Claypool et al., 1980). Calculations for the above diagram are based on equations given by Ohmoto and Goldhaber (1997, p. 529).

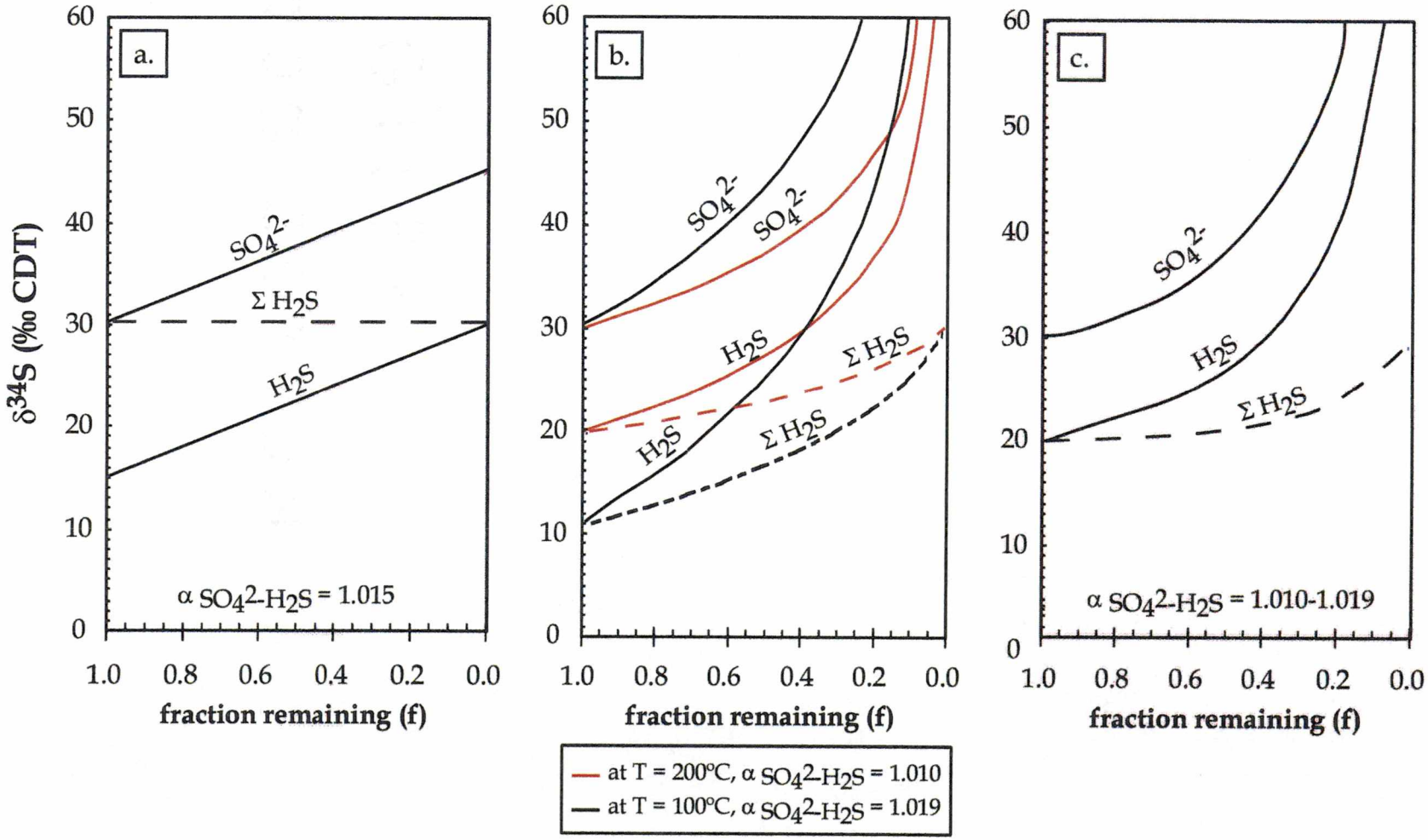
a.
b.
c.
$\delta^{34}S$ (‰ CDT)
60
50
40
30
20
10
0
1.0
0.8
0.6
0.4
0.2
0.0
fraction remaining (f)
SO_4^{2-}
ΣH_2S
H_2S
α SO_4^{2-}-H_2S = 1.015
α SO_4^{2-}-H_2S = 1.010-1.019
— at T = 200°C, α SO_4^{2-}-H_2S = 1.010
— at T = 100°C, α SO_4^{2-}-H_2S = 1.019

10‰ to 50‰, including lower $\delta^{34}S$ values than those noted in either in the present study or that of Jones (1993). The range of $\delta^{34}S$ (sphalerite) values noted in this study can be produced by Rayleigh fractionation at an initial temperature of 200°C ($\alpha_{SO4\text{-}H2S}$ = 1.010). It is unlikely that the temperature will remain constant throughout sphalerite precipitation and fluid inclusion data indicate a range of temperatures from 85° to 197°C. Figure 17c illustrates the effect of a hypothetical temperature decrease from 200° to 100°C and the subsequent effect on $\delta^{34}S$. However, Rayleigh fraction is unidirectional process that cannot account for the observed microscale variations in $\delta^{34}S$ (sphalerite).

In summary, the high $\delta^{34}S$ (sphalerite) values obtained in this study may be related to TSR of high and variable $\delta^{34}S$ at the site of deposition. The genetic model proposed below, therefore, envisages transport of high-$\delta^{34}S$ sulfate to the depositional site along with the metal-bearing fluid and thermochemical reduction of the sulfate by a gas cap at the depositional site.

Proposed Genetic Model

The precipitation model must explain microscale isotopic variations within single thin sections, the wide range of $\delta^{34}S$ values reported for the MJC district, and the very high $\delta^{34}S$ values that have not been observed in other MVT districts. The model invoked to explain the observed $\delta^{34}S$ values requires the transport of metals (most likely as chloride complexes) and sulfate in the same solution and the presence of a gas cap providing CH_4 and lesser amounts of H_2S

at the site of deposition for sulfide precipitation. The sour gas cap provided CH_4 and some H_2S that reside in the high porosity areas of the breccia bodies. The migrating brine carried metal complexes and sulfate together. By contact with the CH_4 in the gas cap, the sulfate would be reduced by thermochemical reduction to produce H_2S that would immediately precipitate sulfide minerals. Some of the H_2S with $\delta^{34}S$ of ~15-30‰ provided by the gas cap would also precipitate sulfide minerals and account for the $\delta^{34}S$ (sphalerite) values at the lower end of the spectrum. The fluid flow in Mississippi Valley-type deposits is episodic in nature (Cathless and Smith, 1983) and each pulse of fluid may have a slightly different metal content and $\delta^{34}S$ (sulfate) depending on the source and any partial reduction of the sulfate reservoir that may have occurred prior to or during transport. The mixing in various proportions of two fluids of variable $\delta^{34}S$ composition could produce the microscale variations noted in the samples.

The bulk of sulfur in this system was likely provided by the dissolved sulfate in the mineralizing fluid rather than the H_2S in the gas cap. Sulfate reduction is a slower process at the relatively low temperatures inferred for the MJC district, and the precipitation of sulfides due to mixing with pre-existing H_2S should be a relatively rapid process in comparison. If pre-existing H_2S dominated the system at the depositional site, sulfide mineral precipitation should have occurred rapidly, resulting in very fine-grained sphalerite, which is not the dominant texture of sphalerite in the MJC district. Additionally, some

H_2S of the sour gas cap may have been removed by early pyrite precipitation. Thus, reduction of sulfate brought by the mineralizing solution is inferred to have been the most likely process responsible for sphalerite mineralization.

If fluid temperatures were lower than about 200°C, the source of sulfate would need to be enriched relative to seawater sulfate (~30‰) to produce sulfide minerals with $\delta^{34}S$ values from 20‰ to 51‰. The source of this enriched sulfate is not immediately obvious. However, one possibility is partial sulfate reduction (by TSR or BSR) in a system closed to SO_4^{2-} but open to H_2S would cause the remaining sulfate to be enriched in ^{34}S.

Chapter Six

Conclusions

In this study, we have used the ion microprobe to determine the fine-scale (20-30μm) sulfur isotopic variations associated with sphalerite from the MVT deposits from the Mascot-Jefferson City zinc district, East Tennessee. These *in situ* sulfur isotopic analyses of sphalerite from deposits that span most of the Mascot-Jefferson City district shows the widest range and heaviest $\delta^{34}S$ values (20.2‰ to 51.0‰) ever reported for these deposits, as well as significant microscale variations.

1. Two textural varieties of sphalerite were noted – zoned and unzoned, as well as two generations of pyrite. The unzoned sphalerite has the lightest $\delta^{34}S$ values (20.2‰ to 39.5‰), the highest Fe contents (0.2-7.63 wt. %), and lowest Cd contents (0-0.37 wt. %), whereas color banded sphalerite is generally zoned, has high concentrations of organic carbon, the heaviest $\delta^{34}S$ values (27.8‰ to 51.0‰), lowest Fe contents (0.03-0.32 wt. %), and highest Cd contents (0.03-0.96 wt. %). Diagenetic pyrite has very light $\delta^{34}S$ values (–16‰ to -21‰) and is earlier than sphalerite mineralization. Main ore stage pyrite has $\delta^{34}S$ values ranging from 31.3‰ to 33.7‰ which is only ~2-6‰ different than adjacent sphalerite.

2. Temperature estimates from fluid inclusion microthermometry and sulfur isotope geothermometry provide similar temperature values. This study found fluid inclusion homogenization temperatures of 140±54°C (139.2°C average). The

sulfur isotope geothermometry equation of Ohmoto and Rye (1986) yields temperature estimates of 149±31°C.

3. The most reasonable mechanism is a sulfate- and metal-bearing brine, which came into contact with an H_2S-rich gas cap, thereby initiating sulfate reduction and precipitation of metal sulfides. The sulfur in the fluid dominated sulfide mineralization, and each pulse of fluid may have has a slightly different $\delta^{34}S$ (SO_4^{2-}) value. Mixing of H_2S in the gas cap with H_2S provided by reduction of sulfate in the fluid would provide the $\delta^{34}S$ variability noted in microanalysis. H_2S in the gas cap likely had a $\delta^{34}S$ value similar to that of seawater sulfate, if the sulfate reduction was nearly complete (~26‰ to 34‰).

References

Anderson, G. M., 1973, The hydrothermal transport and deposition of galena and sphalerite near 100 degrees C: Economic Geology, 68, 480-492.

Anderson, G. M., 1975, Precipitation of Mississippi Valley-type ores: Economic Geology, 70, 937-942.

Anderson, G. M., 1983, Some geochemical aspects of sulfide precipitation in carbonate rocks, In: International Conference on Mississippi valley-type lead-zinc deposits; proceedings volume, Kisvarsanyi, G. ed., 61-76

Anderson, G. M., 1991, Organic maturation and ore precipitation in Southeast Missouri: Economic Geology, 86, 909-926.

Anderson, G. M. and MacQueen, R. W., 1982, Ore deposit models; 6 Mississippi Valley-type lead-zinc deposits: Geoscience Canada, 9, 108-117.

Appold, M. S., Kesler, S. E., Alt, J.C., 1995, Sulfur isotope and fluid inclusion constraints on the genesis of Mississippi valley-type mineralization in the central Appalachians: Economic Geology, 90,909-919.

Bachinski, D. J., 1969, Bond strength and sulfur isotopic fractionation in coexisting sulfides: Economic Geology, 64, 56-65.

Barnes, H. L., 1983, Ore-depositing reactions in Mississippi valley-type deposits, In: International Conference on Mississippi valley-type lead-zinc deposits; proceedings volume, Kisvarsanyi, G. ed., 77-85.

Barton, P. B., 1967, Possible role of organic matter in the precipitation of the Mississippi valley ores: Economic Geology Monographs, 371-377.

Beales, F. W., 1975, Precipitation mechanisms for Mississippi Valley-type ore deposits: Economic Geology, 7, 943-948.

Caless, J. R., 1983, Geochemistry and paragenesis of sphalerite mineraliztion in the East Tennessee zinc district: Unpublished Ph.D. dissertation, Virginia Polytechnic Institute.

Cathles, L. M., and Smith, A. T., 1983, Thermal constraints on the formation of Mississippi valley-type lead-zinc deposits and their implications for episodic basin dewatering and deposit genesis: Economic Geology, 78, 983-1002.

Churnet, H. G., and Misra, K. C., 1983, Sphalerite mineralization and its relationship to carbonate facies boundaries, Copper Ridge District, East Tennessee, In: International Conference on Mississippi valley-type lead-zinc deposits; proceedings volume, Kisvarsanyi, G. ed., 360-372.

Churnet, H. G., Misra, K.C., and Walker, K.R., 1982, Deposition and dolomitization of upper Knox carbonate rocks, Copper Ridge district, east Tennessee: Geological Society of America Bulletin, 93, 76-86.

Claypool, G. E., Holser, W. T., Kaplan, I. R., Sakai, H, Zak, I., 1980, The age curves of sulfur and oxygen isotopes in marine sulfate and their mutual interpretation: Chemical Geology, 28, 3-4, 19-260.

Craig, J. R., Solberg, T. N., and Vaughan, D. J., 1983, Growth characteristics of sphalerites in Appalachian zinc deposits, In: International Conference on Mississippi valley-type lead-zinc deposits; proceedings volume, Kisvarsanyi, G. ed., 317-327.

Crawford, J., Fulweiler, R. E., and Miller, H. W., 1969, Mine geology of the New Jersey Zinc Company's Jefferson City mine: Papers on the stratigraphy and mine geology of the Kingsport and Mascot Formations (Lower Ordovician) of East Tennessee: Tennessee Division of Geology Report of Investigations, 23, 64-75.

Crocetti , C. A. and Holland, H. D., 1989, Sulfur-lead isotope systematics and the composition of fluid inclusions in galena from the Viburnum Trend, Missouri: Economic Geology, 84, 2196-2216.

Crowe, D. E. and Vaughan, R. G., 1996, Characterization and use of isotopically homogeneous standards for in situ laser microprobe analysis of $^{34}S/^{32}S$ ratios: American Mineralogist, 81, 187-193.

Cumming, G. L., and Robertson, D. K., 1969, Isotopic composition of lead from the Pine Point deposit: Economic Geology, 64, 731-732.

Deloule E., Allegre, C. and Doe, B., 1986, Lead and Sulfur Isotope Microstratigraphy in Galena Crystals from Mississippi Valley-type Deposits: Economic Geology, 81, 1307-1321.

Ebers M. L. and Kopp, O. C., 1979, Cathodoluminescent microstratigraphy in gangue dolomite, the Mascot-Jefferson City District, Tennessee: Economic Geology, 74; 4, 908-918.

Fayek, M and Kyser, T. K., 2000, Low temperature oxygen isotopic fractionation in the uraninite --UO (sub 3) -CO (sub 2) -H (sub 2) O system: Geochimica Cosmochimica Acta, 64; 2185-2197.

Foley, N. K., 1980, Mineralogy and geochemistry of the Austinville-Ivanhoe district, Wythe County, Virginia: M.S. Thesis, Virginia Polytechnic Institute and University.

Foley N. K., Sinha, A. K., and Craig, J. R., 1981, Isotopic composition of lead in the Austinville-Ivanhoe Pb-Zn district, Virginia: Economic Geology, 76, 2012-2017.

Garven, G., and Freeze, R. A., 1984, Theoretical analysis of the role of groundwater flow in the genesis of stratabound or deposits; 1, Mathematical and numerical model: American Journal of Science, 284, 10, 1085-1124.

Garven, G., 1985, The role of regional fluid flow in the genesis of the Pine Point Deposit, Western Canada sedimentary basin: Economic Geology, 80, 307-324.

Giordano, T. H., 1985, A preliminary evaluation of organic ligands and metal-organic complexing in Mississippi valley-type ore solutions: Economic Geology, 80, 96-106.

Giordano, T. H. and Barnes, H. L., 1979, Ore solution chemistry VI; PbS solubility in bisulfide solutions to 300 degrees C: Economic Geology, 74, 1637-1646.

Gize, A. P. and Barnes, H. L., 1987, The organic geochemistry of two Mississippi valley-type lead-zinc deposits: Economic Geology, 82, 457-470.

Harris, L. D., 1969, Kingsport Formation and Mascot Dolomite (Lower Ordovician) of East Tennessee: Tennessee Division of Geology Report Investigations, 23, 1-39.

Harris, L. D., 1971, A Lower Paleozoic Paleoaquifer-the Kingsport Formation and Mascot dolomite of Tennessee and Southwest Virginia, Economic Geology: 66, 735-743.

Hatcher, R. D. and Odum, A. L., 1980, Timing of thrusting in the southern Appalachians, U.S.A.: model for orogeny?: Journal of the Geologic Society of London, 37, 321-327.

Haynes, F. M. and Kesler, S. E., 1987, Chemical evolution of brines during Mississippi valley-type mineralization; evidence from East Tennessee and Pine Point: Economic Geology, 82,53-71.

Haynes, F. M., Beane, R. E., and Kesler, S. E., 1989, Simultaneous transport of metal and reduced sulfur, Mascot-Jefferson City zinc district, East Tennessee, evidence from fluid inclusions: American Journal of Science, 289, 8, 994-1038.

Helgeson, H. C., 1970, A chemical and thermodynamic model of ore deposition in hydrothermal systems, In: Fiftieth Anniversary Symposia, Sulfides, Mineralogical Society of America, 3, 155-186.

Hill, W. T., 1971, The geology, applied geochemistry, and drilling results in the Puncheon Camp creek area, Grainger County, Tennessee: Unpublished Ph.D. dissertation, University of Tennessee, Knoxville.

Hoagland, A. D., Hill, W. T., Fulweiler, R. E., 1965, Genesis of the Ordovician zinc deposits in East Tennessee: Economic Geology, 60; 4, 693-714.

Jackson, S. A. and Beales, F. W., 1967, An aspect of sedimentary basin evolution: the concentration of Mississippi Valley-type ores during late stages of diagenesis: Canadian Petroleum Geology Bulletin, 15, 483-522.

Jones, H. D., 1993, Geochemical and sulfur isotopic investigations into the origins of Mississippi Valley-type mineralization in the southern Appalachians and nearby areas: Unpublished Ph.D. dissertation, University of Michigan, Ann Arbor.

Jones, H. D., and Kesler, S. E., 1992, Fluid inclusion gas chemistry in east Tennessee Mississippi valley-type districts, evidence for immiscibility and implications for depositional mechanisms: Geochimica et Cosmochimica Acta, 56, 137-154.

Kesler, S. E., Jones, L. M., and Ruiz, J., 1988, Strontium isotopic geochemistry of Mississippi valley-type deposits, East Tennessee; implications for age and source of mineralizing brines: Geology Society America Bulletin, 100, 1300-1307.

Kesler, S. E., Jones, H. D., Furman, F. C., Sassen, R., Anderson, W. H. and Kyle, J. R., 1994, Role of crude oil in the genesis of Mississippi Valley-type deposits; evidence from the Cincinnati arch: Geology, 22, 609-612.

Kessen, K. M., Woodruff, M. S., and Grant, N. K., 1981, Gangue mineral (super 87) Sr/(super 86) Sr ratios and the origin of Mississippi valley-type mineralization: Economic Geology, 76, 913-920.

Kettler, R. M., 1990, Organic Matter in Hydrothermal Systems: Implications for fluid chemistry and source: Unpublished Ph.D. dissertation, University of Michigan, Ann Arbor, 169-212.

Kharaka, Y. K., Law, L. M, Carothers, W. W., and Goerlitz, D. F, 1986, Role of organic species dissolved in formation waters from sedimentary basins in mineral diagenesis, In: Roles of organic matter in sediment diagenesis, 38, 111-122.

Kiyosu Y. and Krouse, H. R., 1990, The role of organic acid in the abiogenic reduction of sulfate and the sulfur isotope effect: Geochemical Journal, 24, 21-27.

Layne, G. D., Hart, S. R., Shimizu, N., 1991, Microscale lead and sulfur isotope zonation in hydrothermal sulfides by ion microprobe; new findings from the Mississippi valley-type Pb-Zn deposits of the Viburnum Trend, S. E. Missouri: Geology Society America abstracts, 23, 101-102.

Leshin L. A., McKeegan, K. D., Carpenter, P K., Harvey, R. P., 1998, Oxygen isotopic constraints on the genesis of carbonates from Martian meteorite ALH84001: Geochimica Cosmochimica Acta, 62, 3-13.

Leventhal, J. S., 1990, Organic matter and thermochemical sulfate reduction in the Viburnum Trend, Southeast Missouri: Economic Geology, 85, 622-632.

Lyon I. C., Saxton, J. M., Burley, S. D. Guscott, S., McKeever, P. J., Turner, G., 1994, High spatial resolutions measurements of delta (super 18) O in authigenic quartz overgrowths: Mineral. Magazine, 58A, L-Z, 545-546.G. D.

Machel, H. G., 1989, Relationships between sulphate reduction and oxidation of organic compounds to carbonate diagenesis, hydrocarbon accumulations, salt domes, and metal sulphide deposits: Carbonates and Evaporites 4, 137-151.

Machel, H.G., Krouse, H. R., Sassen, R., 1995, Products and distinguishing criteria of bacterial and thermochemical sulfate reduction: Applied Geochemistry, 10, 373-389.

McCormick, J. E., Evans, L. L., Palmer, R. A., and Rasnick, F. D., 1971, Environment of the zinc deposits of Mascot-Jefferson City district, Tennessee: Economic Geology, 66, 757-762.

McKibben, M. A. and Eldridge, S. C., 1995, Microscopic Sulfur Isotope Variations in Ore Minerals from the Viburnum Trend, Southeast Missouri: A SHRIMP study: Economic Geology, 90, 228-245.

Misra, K. C., 2001, Understanding Mineral Deposits, Kulwer Academic Publishers, Norwell, Massachusetts, p. 604.

Nakai, S., Halliday, A. N., Kesler, S. E., Jones, H. D., 1990, Rb-Sr dating of sphalerites from Mississippi valley type (MVT) deposits, In: Seventh international conference on geochronology, cosmochronology and isotope geology, abstracts volume, Geology Society Australia, Sydney, N.S.W., Australia, 27, 69.

Nakai, S., Halliday, A. N., Kesler, S. E., Jones, H. D., Kyle, J. R., and Lane, T. E., 1993, Rb-Sr dating of sphalerites from Mississippi Valley-type (MVT) ore deposits: Geochimica et Cosmochimica Acta, 57, 417-427.

Ohmoto, H., 1972, Systematics of sulfur and carbon isotopes in hydrothermal ore deposits: Economic Geology, 67, 551-578.

Ohmoto, H., and Rye, R. O., 1979, Isotopes of sulfur and carbon, In: Barnes, H. L., ed., Geochemistry of hydrothermal ore deposits, 2nd ed.: New York, John Wiley & Sons, p. 509-567.

Ohmoto, H. and Goldhaber, M. B., 1997, Sulfur and carbon isotopes, In Barnes, H. L., ed., Geochemistry of hydrothermal ore deposits, 2nd ed., New York John Wiley & Sons, p. 517-612.

Ohmoto, H., 1986, Stable isotope geochemistry of ore deposits. In: Stable isotopes in high temperature geological processes. Valley, J. W., Taylor, H. P., O'Neill, J. R., eds., Mineralogical Society of America. Washington, D.C., Reviews in Mineralogy, 16, 491-599.

Olson, R. A., 1984, Genesis of paleokarst and strata-bound zinc-lead sulfide deposits in a Proterozoic dolostone, northern Baffin Island, Canada: Economic Geology, 79, 1056-1103.

Riciputi, L. R., 1996, A comparison of extreme energy filtering and high mass resolution techniques for the measurement of $^{34}S/^{32}S$ ratios by ion microprobe: Rapid Communications in Mass Spectrometry, 10, 282-286.

Riciputi, L. R., Paterson, B. A., and Ripperdan, R. L., 1998, Measurement of light sable isotope ratios by SIMS: Matrix effects for oxygen, carbon and sulfur isotopes in minerals: International Journal of Mass Spectrometry, 178, 81-112.

Roedder, E. and Dwornik, E. J., 1968, Sphalerite color banding: lack of correlation with iron content, Pine Point, Northwest territories, Canada: American Mineralogist, 53, 1523-1529.

Roedder, E., 1971, Fluid-inclusion Evidence on the Environment of Formation of Mineral deposits of the Southern Appalachian Valley: Economic Geology, 86, 777-791.

Roedder, E., 1984, In: Fluid Inclusions, Reviews in Mineralogy, Washington D.C., Mineralogical Society of America., 12, 644.

Sakai, H., 1968, Isotopic properties of sulfur compounds in hydrothermal processes, Geology Journal, 2, 29-49.

Sangster, D. F., 1983, Mississippi valley-type deposits; a geological mélange, In: International Conference on Mississippi valley-type lead-zinc deposits; proceedings volume, Kisvarsanyi, G. ed., 7-19.

Sasaki, A. and Krouse, H.R., 1969, Sulfur isotopes and the Pine Point lead-zinc mineralization: Economic Geology, 64, 718-730

Shrooer, J. M., Rhodin, T. N., and Bradley, R. C., 1973, A quantum-mechanical model for the ionization and excitation of atoms during sputtering: Surface Science, 34, 571-580.

Shanmugam, G., and Lash, G.G., 1982, Analogous tectonic evolution of the Ordovician foredeeps. southern and central Appalachians: Geology, 10, 562-566.

Shimizu N. and Hart, S. R., 1982, Applications of the ion microprobe to geochemistry and cosmochemistry: Annual Reviews in Earth and Planetary Science., 10, 483-526.

Sverjensky, D. A., 1981, The origin of a Mississippi valley-type deposit in the Viburnum Trend, Southeast Missouri: Economic Geology, 76, 1848-1872.

Sverjensky, D. A., 1984, Oil field brines as ore-forming solutions: Economic Geology, 79, 23-37.

Taylor, M., Kesler, S.E., Cloke, P.L., and Kelly, W.C., 1983, Fluid inclusion evidence for fluid mixing, Mascot-Jefferson City Zinc district, Tennessee: Economic Geology, 78, 1425-1439.

Thode and Monster, 1973, Sulfur isotope geochemistry of petroleum, evaporites, and ancient seas, In: Marine Evaporites; origin, diagenesis and geochemistry, Dowden, Hutchinson & Ross,

Valley J. W., and Graham, C. M., 1991, Ion microprobe analyses of oxygen isotopes in magnetite and ilmenite: Eos, Transactions, American Geophysical Union, 72, 292.

Valley, J. W., Eiler, J. M., Graham, C. M, Gibson, E. K, Jr., and Romanek, C. S., 1997, Ion microprobe analysis of oxygen and carbon isotope ratios in the ALH84001: Lunar and Planetary Science Conference abstracts, 1475-1476.

Walker, K. R. and Foreman, J. L., 1990, Early diagenetic history controls burial alteration; comparison of Cambrian and Ordovician carbonates in the S. Appalachians, U.S.A., In: 13th International Sedimentological Congress, 13; 582.

Williams, G. E., 1979, Sedimentology, stable-isotope geochemistry and paleo-environment of dolostones capping late Precambrian glacial sequences in Australia: Journal of the Geological Society of Australia, 26, 377-386.

Yu, M. L. and Lang, N., 1986, Mechanisms of atomic ion emission during sputtering: Nuclear Instruments and Methods in Physics Research, 14, 403,413.

Zimmerman, R. K. and Kesler, S. E., 1981, Fluid inclusion evidence for solution mixing, Sweetwater (Mississippi Valley-type) district, Tennessee: Economic Geology, 76, 134-142

Appendices

Table A. Sample Descriptions

ID/16/3272 - Jefferson City Mine - Reddish brown massive sphalerite with blocky dolostone.
Sphalerite and dolostone have a mottled texture. Pyrite is very minor in this sample. Has a reddish internal reflectance in plane-polarized light but generally too opaque to note any features.

ID/23/3278 - Jefferson City - Growth banded sphalerite on dolomite substrate.
Without the aid of a microscope the color or growth bands of this sample are evident. Under plane light the color bands are discernable. The sphalerite appeared to grown outward from a dolomite substrate, which is surrounding a finer grain calcite layer. The first band is dark with organic matter. The next bands are alternating between a light yellow, to a darker brown and a lighter brown possibly intermediate in composition between the other bands. There are numerous dark opaque blobs within all the layers, which are most likely organic matter. Individual crystals are hard to discern in the early layers. However, outer later layers have larger and more visible crystals. Under reflected-light the sphalerite appears homogeneous. Backscatter electron imaging does not reveal much difference in the layers. Pyrite crystals are arranged in a linear pattern possibly due to a vein or fracture filling. Large anhedral pyrite adjacent to dolomite and within the sphalerite at the boundary between the two phases. Pyrite appears ragged or chewed up possibly due to a reaction during sphalerite mineralization. Pyrite was not found in sphalerite in any other area of the thin section.

IG/ /3590 - Coy Mine - Rosette with thin band of organic matter.
Color banding is visible without microscope. In plane-polarized light there is a darker yellow sphalerite in the center growing around a small piece of dolomite, which is surrounded by a black band and a light honey yellow sphalerite. The darker yellow sphalerite appears to be smaller crystals. A black opaque band presumably rich in organic matter surrounds this layer. The outer layer of lighter yellow sphalerite consists of larger crystals. Under reflected-light there is no color difference between any of these three layers. Pyrite is included in the black band and crystals are arranged linearly. Pyrite crystals are small (~10μ) across and anhedral.

3579 - Coy Mine - Color zoned sphalerite with sphalerite sediment and white gangue dolomite. This is the same as the picture in Figure 5
There are small (10 mm) rosettes of sphalerite - honey-yellow in center with outer band around all three rosettes. The band is ~1 mm thick and is surrounded by greenish-yellowish sphalerite crystals. The crystals in contact with the organic rich band are smaller and are surrounded by larger greenish yellow sphalerite. Small band of sphalerite sand outward of the sphalerite. There is also white gangue dolomite in the layer outward of sphalerite.

sds-1 - Young Mine - The sample is an example of the sphalerite rosette structures. Without the aid of a microscope the center of honey yellow sphalerite is surrounded by a black band with more of honey yellow sphalerite making up the outermost layer of the rosette. In plane light, the center consists of a fine-grained dark greenish brown sphalerite with small crystals of dolomite. The inner layer is separated from the outer sphalerite by a band of black sphalerite. The dark color and opaque nature of this sphalerite is attributed to the presence of organic matter. The outer sphalerite is a lighter yellow color with larger crystals. Light sphalerite replacing dark sphalerite. It appears that the darker sphalerite was deposited first and later replaced with the lighter sphalerite. In reflected light the entire sample appears homogeneous. Backscatter electron-imaging shows a more mottled appearance in the inner sphalerite and a less mottled appearance in the outer layers.

jp2 - New Market Mine - Vein filling sphalerite between dolomite. Pyrite is minor and appears as small crystals within the dolomite as well as in fractures. In one area the dolomite appears to be being replaced or intergrown with sphalerite.

jp5 - New Market Mine - Open space filling sphalerite. White blocky calcite overgrowth on sphalerite. In some areas it appears that the dolomite has inclusions of sphalerite. The center large crystal in figure 8 has a splotchy internal appearance under reflected light. Under plane light this crystal has a center that is darker than the rest of the sample indicating inclusion of organic matter.

Table A (continued)

jp7 - New Market Mine - Vein filling sphalerite between an area of sphalerite sand and micro-brecciated carbonate. On either side of the sphalerite vein there is a distinct black organic layer. Under reflected light the pyrite grains are noticeable. Pyrite is found within the carbonate layer and between this layer and adjacent sphalerite vein. Within the micro-brecciated carbonate there is dolomite, smaller round calcite grains, and possibly some sphalerite sand grains.

Appendix B – Source of error in SIMS analysis

During analysis with a secondary ionization mass spectrometer (SIMS), secondary ions are focused into a fine beam and used to bombard the surface of the sample. SIMS uses a Cs+ beam on conducting phases such as the sulfides in this study. Advantages to using SIMS include small sample size, in situ analysis thereby preserving textural relationships and high resolution. The disadvantages include the errors associated with sputtering.

Several factors contribute to errors during SIMS analyses, and referred to as instrumental mass fractionation (IMF). The processes responsible include - secondary atom extraction (sputtering) and ionization, (e.g., Williams, 1979, Yu and Lang, 1986), secondary ion transmission (Shimizu and Hart, 1982), and detection (Valley and Graham, 1991, Lyon et al., 1994). The greatest contributors to the IMF are sputtering and ionization which depend most strongly upon sample characteristics (i.e., chemical composition). Sputtering with the primary beam produces numerous secondary ions and atomic ions that interfere with the ions of interest (Hoefs, 1990).

Measurement of isotopic ratios by the ion microprobe introduces a certain mass bias in which the light isotope is favored over the heavy isotope. The mass bias may be 10's or 100's ‰ for some elements, but for sulfides the mass bias ranges from 3 to 8 ‰ depending on the secondary ion energy (Riciputi, 1996).

Another error introduced during analysis is referred to as compositionally dependent fractionations or "matrix effects" (e.g., Valley et al., 1997). The matrix effect is related to the in homogeneities in the chemical composition of the mineral and affects the measured isotopic ratios. One way to combat this effect is by careful selection of matrix matched standards. However, finding chemically similar and homogenous standards is often difficult. The use of the Cs+ primary ion beam minimizes the magnitude of the matrix effect (Riciputi, 1996).

Extreme energy filtering (see review by Riciputi, 1996) uses secondary ions with high initial kinetic energies (> 300 keV). This reduces the proportion of hybride species relative to atomic species. Extreme energy filtering allows operation at low mass resolution thereby simplifying instrument tuning.

To correct for the errors associated with ion microprobe analysis, measurements are compared with measurements from a chemically and isotopically homogenous mineral standard, which is compositionally similar to the unknown. Measured ratios for the standard are compared with the accepted values and a correction factor is calculated which is then applied to unknowns measured during the same analytical period (e.g., Leshin et al., 1998). The standards used in this study were Balmat sphalerite (+14‰ CDT) and Balmat pyrite (+14.6‰ CDT) from the Balmat mine, New York (Crowe et al., 1996).

Table C-1. Average electron microprobe analyses of sphalerite from the Mascot-Jefferson City zinc district

	New Market - jp2													
#	12-2s6		12-2s5		12-2s7		12-2s8		12-2s9		12-2s10		12-2s11	
n[1]	[5]		[2]		[4]		[4]		[4]		[5]		[4]	
Weight Percent														
S	32.5	(4)	32.4	(1)	32.1	(2)	32.7	(2)	32.6	(2)	32.5	(1)	32.7	(3)
Fe	0.10	(0)	0.04	(4)	0.07	(1)	0.20	(4)	0.21	(11)	0.17	(4)	0.17	(9)
Zn	66.0	(3)	66.4	(1)	65.8	(1)	66.7	(1)	66.0	(6)	65.8	(2)	65.8	(3)
Mn	<.03		<.03		<.03		<.03		<.03		<.03		<.03	
Cu	<.03		0.04	(2)	<.03		<.03		<.03		<.03		<.03	
Cd	0.32	(16)	0.45	(22)	0.59	(10)	0.47	(7)	0.41	(10)	0.29	(6)	0.32	(9)
Σ	98.96		99.30		98.66		100.05		99.19		98.78		99.00	
Cations on the basis of 1 mole of sulfur														
Fe	0.002		0.001		0.001		0.004		0.004		0.003		0.003	
Zn	0.996		1.005		1.005		1.000		0.992		0.993		0.989	
Mn	-		-		-		-		-		-		-	
Cu	-		-		-		-		-		-		-	
Cd	0.003		0.004		0.005		0.004		0.004		0.003		0.003	
Σ	2.001		2.010		2.012		2.008		2.000		1.999		1.994	

					New Market - jp7									
#	12-2s13		12-2s14		12-2s33		12-2s32		12-2s31		12-2s30		12-2s36	
n[1]	[4]		[2]		[4]		[5]		[3]		[4]		[3]	
Weight Percent														
S	32.5	(4)	32.6	(2)	32.2	(4)	32.5	(3)	32.7	(6)	32.3	(4)	32.6	(3)
Fe	0.14	(7)	0.09	(0)	0.24	(9)	0.11	(3)	0.15	(5)	0.09	(3)	0.07	(1)
Zn	66.2	(3)	66.2	(4)	66.3	(4)	66.4	(5)	66.2	(1)	66.3	(3)	66.5	(9)
Mn	<.03		<.03		<.03		<.03		<.03		<.03		<.03	
Cu	<.03		<.03		<.03		<.03		<.03		<.03		<.03	
Cd	0.16	(6)	0.25	(5)	0.46	(5)	0.42	(8)	0.45	(7)	0.31	(8)	0.10	(5)
Σ	99.02		99.07		99.25		99.43		99.55		99.02		99.20	
Cations on the basis of 1 mole of sulfur														
Fe	0.003		0.002		0.004		0.002		0.003		0.002		0.001	
Zn	1.000		0.996		1.009		1.003		0.993		1.007		1.001	
Mn	-		-		-		-		-		-		-	
Cu	-		-		-		-		-		-		-	
Cd	0.001		0.002		0.004		0.004		0.004		0.003		0.001	
Σ	2.004		2.000		2.017		2.009		1.999		2.011		2.003	

[1] n equals the number of spot analyses in each average. The number in parentheses represents the one sigma standard deviation in terms of the last digit cited. Sample 12-2s12 data was unusable due to low totals.

Table C-1 (continued)

New Market - jp5													
#	12-2s20		12-2s19		12-2s18		12-2s17		12-2s16		12-2s15		12-2s23	
n[1]	[2]		[3]		[4]		[2]		[2]		[4]		[3]	
Weight Percent														
S	32.2		32.5	(2)	32.3	(2)	32.4	(2)	32.3	(1)	32.4	(2)	32.2	(1)
Fe	0.07		0.10	(1)	0.07	(2)	0.05	(3)	0.04	(0)	0.07	(2)	0.08	(3)
Zn	65.8		66.1	(1)	66.1	(1)	66.1	(1)	65.9	(1)	65.8	(4)	65.9	(2)
Mn	<.03		<.03		<.03		<.03		<.03		<.03		<.03	
Cu	0.03		<.03		<.03		<.03		<.03		0.04	(1)	0.05	(4)
Cd	0.49		0.38	(4)	0.37	(10)	0.44	(26)	0.51	(3)	0.69	(4)	0.33	(19)
Σ	98.54		99.14		98.87		98.97		98.80		99.05		98.65	
Cations on the basis of 1 mole of sulfur														
Fe	0.001		0.002		0.001		0.001		0.001		0.001		0.001	
Zn	1.002		0.998		1.002		1.001		1.001		0.996		1.003	
Mn	-		-		-		-		-		-		-	
Cu	-		-		-		-		-		-		-	
Cd	0.003		0.003		0.003		0.004		0.005		0.006		0.003	
Σ	2.006		2.003		2.007		2.006		2.006		2.003		2.007	

#	12-2s22		12-2s24	
n[1]	[4]		[2]	
Weight Percent				
S	32.1	(2)	32.3	(3)
Fe	0.18	(5)	0.19	(0)
Zn	66.3	(1)	66.4	(1)
Mn	<.03		<.03	
Cu	<.03		<.03	
Cd	0.28	(12)	0.27	(0)
Σ	98.95		99.21	
Cations on the basis of 1 mole of sulfur				
Fe	0.003		0.003	
Zn	1.013		1.008	
Mn	-		-	
Cu	-		-	
Cd	0.002		0.002	
Σ	2.019		2.014	

[1] n equals the number of spot analyses in each average. The number in parentheses represents the one sigma standard deviation in terms of the last digit cited.

Table C-1 (continued)

Jefferson City - sample 3272												
#	12-2s19		12-2s20		12-2s22	12-2s7	12-2s23		12-2s26	12-2s8		
n[1]	[1]		[3]		[1]	[1]	[3]		[1]	[3]		
Weight Percent												
S	32.6		33.1	(3)	32.4	32.6	32.6	(0)	32.6	33.0	(2)	
Fe	1.28		7.60	(0)	3.81	5.67	2.25	(6)	1.99	0.25	(2)	
Zn	64.6		58.5	(3)	62.5	60.4	64.2	(8)	64.4	66.5	(1)	
Mn	<.03		<.03		<.03	<.03	<.03		<.03	<.03		
Cu	0.0697		0.07	(0)	0.08	0.11	0.06	(1)	0.08	0.03	(2)	
Cd	0.18		0.07	(5)	0.04	<.03	0.14	(2)	0.37	0.21	(4)	
Σ	98.662		99.30		98.8153	98.7609	99.2816		99.3907	100.06		
Cations on the basis of 1 mole of sulfur												
Fe	0.023		0.132		0.068	0.100	0.040		0.004	0.004		
Zn	0.973		0.867		0.947	0.908	0.965		0.988	0.988		
Mn	-		-		-	-	-		-	-		
Cu	0.001		0.001		0.001	0.002	0.001		0.001	0.001		
Cd	0.002		0.001		0.000	-	0.001		0.002	0.002		
Σ	1.998		2.001		2.016	2.009	2.007		1.995	1.995		

#	12-2s25		12-2s9	12-2s10	
n[1]	[3]		[1]	[3]	
Weight Percent					
S	32.6	(1)	32.8	32.5	(1)
Fe	0.54	(24)	0.28	2.92	(6)
Zn	65.8	(5)	66.6	63.4	(11)
Mn	<.03		<.03	<.03	
Cu	<.03		0.04	0.04	(4)
Cd	0.25	(7)	0.22	0.12	(1)
Σ	99.1492		99.9291	98.9675	
Cations on the basis of 1 mole of sulfur					
Fe	0.010		0.005	0.052	
Zn	0.991		0.994	0.959	
Mn	-		-	-	
Cu	-		0.001	0.001	
Cd	0.002		0.002	0.001	
Σ	2.003		2.001	2.012	

[1] n equals the number of spot analyses in each average. The number in parentheses represents the one sigma standard deviation in terms of the last digit cited.

Table C-2. Point by point electron microprobe analyses of sphalerite from Mascot-Jefferson City zinc district

	Sample IG/3590								
#	1	2	3	4	5	6	9	10	11
Weight percent									
S	32.3	32.0	32.8	32.3	32.0	32.3	32.8	32.5	32.4
Fe	0.24	0.18	0.17	0.21	0.17	0.35	0.01	0.03	0.14
Zn	66.5	66.5	66.2	66.9	66.5	65.6	66.5	66.1	66.5
Mn	<.03	<.03	<.03	<.03	<.03	<.03	<.03	<.03	<.03
Cu	0.04	0.06	0.11	0.06	0.04	<.03	<.03	<.03	<.03
Cd	0.41	0.40	0.19	0.24	0.20	0.27	0.12	0.03	0.40
Σ	99.47	99.10	99.49	99.71	98.93	98.55	99.46	98.67	99.43
Cations on the basis of 1 mole of sulfur									
S	1.000	1.000	1.000	1.000	1.000	1.000	1.000	1.000	1.000
Fe	0.004	0.003	0.003	0.004	0.003	0.006	0.000	0.001	0.002
Zn	1.010	1.020	0.990	1.014	1.018	0.995	0.994	0.998	1.006
Mn	0.000	0.000	0.000	0.000	0.000	0.000	0.000	0.000	0.000
Cu	0.001	0.001	0.002	0.001	0.001	0.000	0.000	0.000	0.000
Cd	0.004	0.004	0.002	0.002	0.002	0.002	0.001	0.000	0.004
Σ	2.019	2.028	1.996	2.021	2.023	2.003	1.995	1.999	2.012

#	12	13	14	16	17	18	21	24	25
Weight percent									
S	32.7	32.4	32.6	31.6	32.8	32.7	32.5	32.5	32.4
Fe	0.17	0.10	0.14	0.08	0.05	0.11	0.13	0.13	0.14
Zn	66.0	66.2	66.5	66.2	67.0	66.2	66.4	66.1	66.7
Mn	<.03	<.03	0.03	<.03	<.03	<.03	<.03	<.03	<.03
Cu	0.04	<.03	<.03	0.06	<.03	<.03	<.03	0.05	<.03
Cd	0.34	0.25	0.18	0.33	0.20	0.37	0.42	0.13	0.13
Σ	99.32	98.90	99.41	98.19	100.01	99.48	99.41	98.98	99.36
Cations on the basis of 1 mole of sulfur									
S	1.000	1.000	1.000	1.000	1.000	1.000	1.000	1.000	1.000
Fe	0.003	0.002	0.002	0.001	0.001	0.002	0.002	0.002	0.002
Zn	0.991	1.003	1.001	1.028	1.002	0.992	1.002	0.997	1.011
Mn	0.000	0.000	0.001	0.000	0.000	0.000	0.000	0.000	0.000
Cu	0.001	0.000	0.000	0.000	0.000	0.000	0.000	0.000	0.000
Cd	0.003	0.002	0.002	0.003	0.002	0.003	0.004	0.001	0.001
Σ	1.997	2.007	2.005	2.033	2.005	1.998	2.008	2.001	2.015

Table C-2 (continued)

Sample 3278									
#	3	4	5	7	8	9	10	11	12
Weight Percent									
S	32.8	32.8	32.2	32.7	32.6	32.7	32.7	32.6	31.8
Fe	0.25	0.24	0.12	0.28	0.15	0.13	0.36	0.36	0.30
Zn	66.6	66.8	67.5	64.6	67.5	67.5	66.3	66.8	66.6
Mn	<.03	<.03	<.03	<.03	<.03	<.03	<.03	<.03	<.03
Cu	<.03	<.03	<.03	<.03	<.03	<.03	0.0353	<.03	<.03
Cd	0.36	0.32	0.10	0.86	0.13	0.11	0.22	0.20	0.14
Σ	100.02	100.17	99.93	98.51	100.38	100.48	99.68	99.96	98.86
Cations on the basis of 1 mole of sulfur									
S	1.000	1.000	1.000	1.000	1.000	1.000	1.000	1.000	1.000
Fe	0.004	0.004	0.002	0.005	0.003	0.002	0.006	0.006	0.005
Zn	0.994	0.999	1.028	0.968	1.015	1.012	0.993	1.003	1.029
Mn	0.000	0.000	0.000	0.000	0.000	0.000	0.000	0.000	0.000
Cu	0.000	0.000	0.000	0.000	0.000	0.000	0.001	0.000	0.000
Cd	0.003	0.003	0.001	0.008	0.001	0.001	0.002	0.002	0.001
Σ	2.001	2.0063	2.0311	1.9804	2.018	2.016	2.002	2.011	2.035

#	13	14	16	17	19	20
Weight Percent						
S	32.7	32.4	32.3	32.4	32.3	33.0
Fe	0.38	0.28	0.14	0.18	0.09	0.07
Zn	66.0	66.6	67.1	66.0	66.9	67.1
Mn	<.03	<.03	<.03	<.03	0.05	<.03
Cu	<.03	<.03	0.05	0.12	0.19	0.06
Cd	0.28	0.19	0.56	0.60	0.55	0.52
Σ	99.43	99.51	100.09	99.30	100.04	100.69
Cations on the basis of 1 mole of sulfur						
S	1.000	1.000	1.000	1.000	1.000	1.000
Fe	0.007	0.005	0.002	0.003	0.002	0.001
Zn	0.990	1.008	1.020	0.998	1.015	0.997
Mn	0.000	0.000	0.000	0.000	0.001	0.000
Cu	0.000	0.000	0.001	0.002	0.003	0.001
Cd	0.002	0.002	0.005	0.005	0.005	0.005
Σ	1.999	2.015	2.028	2.008	2.025	2.004

Table C-2 (continued)

	Sample 1A/sds1								
#	1	4	5	6	7	8	9	10	11
Weight percent									
S	32.4	32.4	32.3	32.3	32.7	32.0	32.3	32.1	32.0
Fe	0.08	0.03	0.08	0.05	0.07	0.09	0.25	0.09	0.15
Zn	66.2	67.4	66.3	66.6	66.8	66.6	66.4	66.7	66.6
Mn	<.03	<.03	<.03	<.03	<.03	<.03	<.03	<.03	<.03
Cu	<.03	0.15	0.06	<.03	0.09	0.03	0.05	<.03	0.07
Cd	0.57	0.25	0.54	0.10	0.49	0.20	0.36	0.53	0.75
Σ	99.25	100.19	99.30	99.03	100.16	98.97	99.39	99.44	99.55
Cations on the basis of 1 mole of sulfur									
S	1.000	1.000	1.000	1.000	1.000	1.000	1.000	1.000	1.000
Fe	0.001	0.001	0.001	0.001	0.001	0.002	0.005	0.002	0.003
Zn	1.001	1.020	1.005	1.010	1.001	1.019	1.007	1.020	1.019
Mn	0.000	0.000	0.000	0.000	0.000	0.000	0.000	0.000	0.000
Cu	0.000	0.002	0.001	0.000	0.000	0.000	0.001	0.000	0.000
Cd	0.005	0.002	0.005	0.001	0.004	0.002	0.003	0.005	0.007
Σ	2.007	2.025	2.012	2.012	2.006	2.023	2.015	2.027	2.028

#	12	13	14	15	16	17	18	19	20
Weight percent									
S	32.8	32.0	32.3	32.3	32.6	32.2	32.3	31.7	32.5
Fe	0.07	0.08	0.30	0.18	0.32	0.16	0.12	0.10	0.09
Zn	66.3	66.6	66.7	66.3	65.5	66.5	66.3	66.4	66.6
Mn	<.03	<.03	<.03	<.03	<.03	0.05	<.03	<.03	<.03
Cu	<.03	<.03	0.15	0.09	0.03	0.14	0.10	0.09	<.03
Cd	0.35	0.29	0.61	0.62	0.96	0.55	0.65	0.44	0.66
Σ	99.51	98.91	99.99	99.54	99.44	99.62	99.48	98.70	99.76
Cations on the basis of 1 mole of sulfur									
S	1.000	1.000	1.000	1.000	1.000	1.000	1.000	1.000	1.000
Fe	0.001	0.001	0.005	0.003	0.006	0.003	0.002	0.002	0.002
Zn	0.990	1.022	1.014	1.006	0.985	1.011	1.006	1.028	1.006
Mn	0.000	0.000	0.000	0.000	0.000	0.001	0.000	0.000	0.000
Cu	0.000	0.000	0.002	0.001	0.000	0.002	0.002	0.001	0.000
Cd	0.003	0.003	0.005	0.005	0.008	0.005	0.006	0.004	0.006
Σ	1.995	2.026	2.027	2.016	1.999	2.022	2.015	2.035	2.013

Table C-2 (continued)

	Sample 1A/sds1								
#	21	23	24	25	26	27	28	29	30
Weight percent									
S	32.8	32.5	31.9	32.4	32.5	32.9	32.5	32.2	32.5
Fe	0.12	0.12	0.09	0.07	0.06	0.07	0.08	0.02	0.06
Zn	66.1	66.7	66.6	65.8	66.4	67.1	66.6	66.4	67.0
Mn	<.03	<.03	<.03	0.04	<.03	<.03	<.03	0.03	<.03
Cu	0.04	<.03	0.11	0.06	<.03	<.03	0.04	0.08	0.03
Cd	0.93	0.47	0.18	0.73	0.23	0.41	0.18	0.18	0.27
Σ	100.00	99.78	98.91	99.10	99.24	100.44	99.36	98.98	99.79
Cations on the basis of 1 mole of sulfur									
S	1.000	1.000	1.000	1.000	1.000	1.000	1.000	1.000	1.000
Fe	0.002	0.002	0.002	0.001	0.001	0.001	0.001	0.000	0.001
Zn	0.990	1.007	1.022	0.995	1.002	1.002	1.005	1.010	1.012
Mn	0.000	0.000	0.000	0.001	0.000	0.000	0.000	0.001	0.000
Cu	0.001	0.000	0.002	0.001	0.000	0.000	0.001	0.001	0.000
Cd	0.008	0.004	0.002	0.006	0.002	0.002	0.002	0.002	0.002
Σ	2.001	2.013	2.027	2.004	2.005	2.005	2.008	2.014	2.016

#	31	32
Weight percent		
S	32.7	32.3
Fe	0.11	0.18
Zn	66.1	66.1
Mn	<.03	<.03
Cu	<.03	<.03
Cd	0.21	0.57
Σ	99.16	99.19
Cations on the basis of 1 mole of sulfur		
S	1.000	1.000
Fe	0.002	0.003
Zn	0.992	1.004
Mn	0.000	0.000
Cu	0.000	0.000
Cd	0.002	0.005
Σ	1.996	2.012

Table D. Sulfur isotope anaylses in sphaleriteby sample and pyrite from Mascot-Jeffeson City district

Location	Analysis #	Description	34/32 meas.	$\delta^{34}S$ (CDT)	1 σ
New	12-2s5	near rim	4.4937	31.2	0.6
Market	12-2s6	rim	4.509	34.8	0.6
jp2	12-2s7	core	4.4786	27.8	0.6
	12-2s8	core	4.4930	31.1	0.6
	12-2s9	next out	4.4940	31.3	0.6
	12-2s10	next out	4.5072	34.3	0.6
	12-2s11	midway	4.4996	32.6	0.6
	12-2s12	near rim	4.5088	34.7	0.6
	12-2s13	rim	4.4931	31.1	0.6
	12-2s14	rim	4.4956	31.7	0.6
New	12-2s15	core	4.4731	26.5	0.6
Market	12-2s16	near to rim	4.4897	30.3	0.6
jp5	12-2s17	m	4.4839	29.0	0.6
	12-2s18	next out	4.5149	36.1	0.6
	12-2s19	rim	4.5082	34.6	0.7
	12-2s20	rim	4.5297	39.5	0.7
	12-2s21	rim	4.4924	30.9	0.7
	12-2s22	medium	4.4872	29.8	0.6
	12-2s23	next in	4.4961	31.8	0.6
	12-2s24	rim	4.5063	34.1	0.7
New	12-2s30	core	4.4891	30.2	0.8
Market	12-2s31	next out	4.4973	32.1	0.6
jp7	12-2s32	rim	4.5033	33.4	0.6
	12-2s33	rim adj pyr	4.5028	33.3	0.7
	12-2s36	other rim	4.4871	29.7	0.8
	12-2s34	lg. groundmass pyrite	4.2415	-16.1	0.4
	12-2s35	sm. groundmass pyrite	4.2249	-20.0	0.4
Jefferson	12-3s7	near rim	4.4407	20.2	1.0
City	12-3s8	around rim	4.4790	29.0	0.5
3272	12-3s9	near rim	4.4633	25.4	0.6
	12-3s10	rim	4.4661	26.0	0.5
	12-3s12	core	4.4469	21.6	0.5
	12-3s13	core	4.4652	25.8	0.6
	12-3s14	core	4.4924	25.1	0.5
	12-3s15	core	4.4534	23.1	0.5
	12-3s16	core	4.4563	23.7	0.6
	12-3s17	heading to rim	4.4551	23.5	0.5
	12-3s18	next	4.4514	22.6	0.6
	12-3s19	next	4.4862	30.6	0.5

Table D (continued)

Location	Analysis #	Description	34/32 meas.	$\delta^{34}S$	1 σ
Jefferson	12-3s20	next	4.4715	27.2	0.6
City	12-3s21	next	4.4488	22.0	0.6
3272	12-3s22	next	4.4493	22.1	0.6
(con't)	12-3s23	between s7&s8	4.4529	23.0	0.5
	12-3s24	adj to s23	4.4558	23.6	0.6
	12-3s25	between s8&s9	4.4754	28.1	0.5
	12-3s26	rim	4.4554	23.5	0.6
	12-3s27	rim	4.4760	28.3	0.6
	12-3s28	rim as 12-3s18	4.4578	24.3	0.7
	12-3s29	little further out	4.4558	23.6	0.6
	12-3s30	back around core	4.4564	23.8	0.6
	12-3s11	groundmass pyrite	4.4348	18.8	0.5
Young	1-19s9	center rosette sp1	4.2964	49.6	1.1
Mine	1-19s21	center rosette out, sp1a	4.4194	50.2	1.0
sds1	1-19s10	next out sp2	4.2385	35.5	1.4
	1-19s22	sp2a	4.3528	34.4	1.1
	1-19s11	next out sp3	4.3021	51.0	1.3
	1-19s23	sp3a	4.3829	41.6	1.9
	1-19s12	next to bl. band, 4	4.2474	37.7	1.5
	1-19s13	black band, 5	4.2543	39.4	1.1
	1-19s14	black band 6	4.2656	42.1	1.1
	1-19s15	outer sphal. 7	4.2480	37.8	1.0
	1-19s16	outermost sphal. 8	4.3014	50.9	1.0
Coy	1-19s27	near dol., 1	4.3641	32.7	0.6
Mine	1-19s28	mid, 2	4.3792	36.2	0.7
3590	1-19s29	pyrite 3	4.4530	31.3	0.5
	1-19s30	pyrite 4	4.4634	33.7	0.4
	1-19s31	near edge, 5	4.3611	32.0	0.7
	1-19s32	at edge, 6	4.3805	36.5	0.6
Jefferson	1-19s37	pyrite, 1	4.4567	32.2	0.4
City	1-19s38	same pyrite, 2nd point	4.4583	32.6	0.5
3278	1-19s39	sph. 3, band 1	4.3917	39.2	0.5
	1-19s40	sph. 4, band 2	4.3683	33.7	0.6
	1-19s41	sph. 5, band 3	4.3720	34.5	0.5
	1-19s42	sph. 6, band 4	4.3628	32.4	0.5
	1-19s43	sph. 7, band 5	4.3436	27.8	0.6
	1-19s44	sph. 8, band 6	4.3909	39.0	0.5
	1-19s45	sph. 9, band 7	4.4112	43.8	0.5

Table E. Fluid Inclusion Freezing and Homogenization Temperatures for sphalerite from Mascot-Jefferson City zinc district

Location	Sample	type	color	Freezing Temperature Tm	Homogenization Temperature Th
Coy Mine	3579	zoned	light	-19.8	100.2
	3579		dark	-20.2	122.7
	3579		dark	-21.5	116.3
	3579		light	-11.7	171.6
	3579		dark	-10.9	187.1
	3579		dark	-35.7	101.4
	3579		light	-14.3	174.9
Coy Mine	3590	rosette	light	-16.2	155.0
	3590		light	-37.1	87.5
	3590		light	-9.2	193.8
	3590		light	-20.6	137.0
	3590		light	-32.5	91.8
	3590		light	-27.4	85.9
	3590		light	-34.0	98.3
	3590		light	-28.3	100.5
Jefferson	3278	zoned	light	-27.1	109.5
City	3278		dark	-7.3	182.0
	3278		dark	-8.0	160.8
	3278		dark	-18.9	147.1
	3278		light	-26.4	104.2
	3278		dark	-23.1	122.7
	3278		light	-37.4	87.3
	3278		light	-39.8	85.6
	3278		dark	-22.5	160.5
	3278		light	-19.8	181.8
	3278		dark	-17.0	109.9
	3278		dark	-8.8	189.4
	3278		dark	-21.8	146.6
	3278		light	-35.6	111.5
	3278		dark	-19.4	126.1
	3278		light	-24.2	128.9
New	jp5	unzoned	light	-10.5	184.5
Market	jp5		light	-24.8	169.0
	jp5		light	-21.3	154.0
	jp5		light	-17.5	170.0
	jp2	unzoned	light	-12.1	172.6
	jp2		light	-34.2	89.6
	jp2		light	-25.1	113.0
	jp2		light	-19.6	161.9
	jp2		light	-13.5	172.9
	jp2		light	-16.0	169.7

Table E. (continued)

Location	Sample	type	color	Freezing Temperature Tm	Homogenization Temperature Th
	jp7	unzoned	light	-26.6	123.2
New	jp7		light	-19.5	159.8
Market	jp7	unzoned	light	-32.7	100.7
	jp7		light	-15.6	194.5
	jp7		light	-24.8	159.9
	jp7		light	-14.6	170.0

Vita

Janna Peevler was born and raised in Augusta Georgia. As a teen her family moved to Watkinsville, Georgia where she graduated from Oconee County High School in 1991. She was steered toward geology by a high school teacher, Mrs. Soutar. After graduation in 1991, she enrolled in nearby University of Georgia in Athens where she began studies in accounting. The brief stint in accounting was sidetracked by an introductory geology class that sparked her interest. In 1996 she received a Bachelor of Science degree in Geology. A year after graduation she enrolled in the University of Tennessee in Knoxville. She has been working with Dr. Kula Misra for several years on Mississippi Valley-type deposits. Future plans include possible employment in the environmental field.